2015

Multiscale Modeling of Particle Transport in Petroleum Reservoirs

Layne Bryan French
Louisiana State University and Agricultural and Mechanical College

MULTISCALE MODELING OF PARTICLE TRANSPORT IN PETROLEUM RESERVOIRS

A Thesis

Submitted to the Graduate Faculty of the
Louisiana State University and
Agricultural and Mechanical College
in partial fulfillment of the
requirements for the degree of
Master of Science

in

The Craft and Hawkins Department of Petroleum Engineering

by
Layne B. French Jr.
B.S., The University of Texas at Austin, 2013
August 2015

ACKNOWLEDGEMENTS

I would like to thank my advisor Dr. Karsten Thompson for his guidance and assistance in completing this project. I have benefitted from his mentorship and willingness to share knowledge of a sophisticated field of study. I would also like to thank the members of my committee Dr. Richard Hughes and Dr. Mehdi Zeidouni for showing interest in the project and offering feedback on my document and presentations. In addition, I'd like to thank Dr. Mayank Tyagi for his attendance and feedback at my thesis proposal and the programming skills I acquired in his classes. I'd like to thank Dr. Yin Feng for working with me to couple the network model with the reservoir simulator that he developed.

This work was funded by the Advanced Energy Consortium (AEC). Once again I thank Dr. Karsten Thompson and Dr. Richard Hughes for including me on the AEC project with Dr. Yin Feng and Paula Sanematsu. I also express thanks to all of the companies funding the AEC. I would like to thank everyone involved with organizing the biannual project review conferences for the AEC and giving us a chance to share our work with the companies and universities involved.

I am thankful for the help I have had from fellow graduate students including Tim Thibodeaux, John Blears, Paula Sanematsu and Godfrey Mills. Without Tim, I would still be trying to compile my first FORTRAN code.

Finally, I would like to thank my parents and sister for the love, support, and education that they have provided me throughout my life. I thank my fiancé for the patience, emotional support, and assistance that she provided for the past two years at a long distance.

TABLE OF CONTENTS

LIST OF TABLES

LIST OF FIGURES

ABSTRACT

Modeling subsurface particle transport and retention is important for many processes, including sand production, fines migration, and nanoparticle injection. In this study, a pore-scale particle plugging simulator is concurrently coupled with a streamline reservoir simulator to predict the behavior of particles in the subsurface. The coupled simulators march forward in time together. The automated communication between the two models enables the prediction of spatially and time dependent parameters that control the particle transport process. At each time step, the reservoir simulator provides the inlet velocity and particle concentration of the fluid suspension to the pore-scale model which outputs the permeability, porosity, and retention coefficient. This permits the reservoir simulator to include pore-scale physics at selected locations to determine the number of particles retained and the formation damage. The pore-scale simulator tracks the path of individual particles as they are simultaneously injected into the sample and produces an effluent particle concentration curve that is fit with a continuum-scale advection-dispersion model. The advection-dispersion model is matched to the pore-scale data by adjusting two parameters: the dispersion and retention coefficient. The retention coefficient dictates the number of particles retained across a grid block in the reservoir simulator. Incorporating fundamental pore-scale physics into the streamline reservoir simulator improves its predictive ability by updating the particle retention and formation damage of a grid block at each time step.

CHAPTER 1. INTRODUCTION

Many processes in the petroleum engineering industry involve particle transport in oil and gas reservoirs including sand production, fines migration, and nanoparticle injection. In these processes it is important to understand where the particles are travelling in the reservoir and the impact that they have on the formation properties. Large particles can damage the formation and decrease permeability which reduces the productive capacity of the reservoir. During nanoparticle injection, forces at the pore level can cause retention of particles and prevent their recovery. In addition, due to the heterogeneity of typical reservoirs, it is difficult to predict how particles will spread across the formation. Determining the fate of particles traveling through petroleum reservoirs requires an extensive knowledge of particle transport behavior in porous media.

Particle transport in porous media is controlled by pore-scale physics. A particle is transported from pore to pore until it reaches an outlet, the fluid in which it is suspended stops flowing, or the particle becomes stuck in the porous medium. A particle can take many different paths through the vast network of pores and fractures that may exist in a petroleum reservoir. Particle transport is affected by the shape of the particles and their surface properties, the structure of the porous medium, the chemistry of the suspending fluid, the flow velocity field in the pore space, and a variety of interaction forces between the particle and the medium (Imdakm and Sahimi, 1991). The factors listed that influence particle transport exist at microscopic scales; therefore the process must be studied at these small scales in order to fully understand and quantify them.

Particle transport has been studied using analytical and empirical equations, experiments, and numerical simulation. This thesis focuses on the use of numerical simulation to gain an understanding of the particle transport process. Particle transport simulation has been conducted at the pore, core, continuum, and field scale (Rhodes and Blunt, 2006). At the continuum-scale, particle suspension transport is typically modeled using various modified forms of the advection-dispersion equation, including the classical colloid filtration theory model (CFT). At the pore-scale particle transport is modeled using a network model or the application of CFD techniques at the pore-scale. As stated above, the pore-scale structure of porous media has a strong influence on the prediction of particle transportation at the field scale. Therefore, successful modeling of particle transport at the field scale requires the incorporation of pore-scale physics. This thesis presents a method for concurrently coupling a pore-scale network model with a continuum-scale reservoir simulator to study the transport and retention of particles in petroleum reservoirs.

Pore network models (Fatt, 1956) define the void structure of the porous medium as a network of interconnected spheres and tubes. The spheres represent the pore chambers while the tubes represent the flow constriction between the chambers. The 3-D network model used in this study was generated from a microtomographic image of a Berea Sandstone sample. The particle injection algorithm can be used to track particles individually as they travel through the network and determine the permeability damage and porosity reduction incurred by a trapped particle. Mechanical straining or size exclusion of particles is the only retention mechanism considered in this model, which is referred to as the particle plugging network model.

The continuum-scale reservoir simulator, developed by a collaborator (Dr. Yin Feng), determines the macroscopic streamlines within the reservoir. It uses a finite difference scheme based on the advection-dispersion equation to determine the change in concentration of a particle suspension along a streamline. To determine the change in concentration along a streamline, the model requires a particle dispersion and retention coefficient. For stand-alone use of the reservoir simulator, these parameters are based on empirical equations or tabulated data. To improve the predictive power of the reservoir simulator, we aim to couple the field-scale model with the particle plugging network model to determine the spatially and time dependent dispersion and retention coefficients and report current values to the simulator during a simulation.

The dispersion and retention coefficient are determined by fitting the classical colloid filtration theory (CFT) model to the effluent concentration data produced by the particle plugging network model. The model is fit using an optimization algorithm to determine the dispersion and retention coefficients that yield the minimum error between the CFT effluent curve and the network model effluent curve. The dispersion and retention coefficient can be determined for any number of particle species (different particle sizes or concentrations). By using the method outlined above, the pore-scale network model can provide time-dependent continuum-scale parameters to the reservoir simulator that dictate the change in concentration across a reservoir streamline.

Previously, pore-scale models have been used in a preprocessing step to determine continuum-scale parameters like the dispersion and retention coefficients. However, this approach offers few advantages over using experimentally obtained parameters and fails to capture dynamic behavior of the continuum-scale parameters. The concurrent coupling approach embeds a network model in one or more gridblocks of the reservoir simulator and the two models march forward in time and exchange information at each time step (Sheng and Thompson, 2013). In this approach, the reservoir simulator passes the boundary conditions to the network model which determines the continuum-scale parameters (permeability, porosity, dispersion coefficient, and retention coefficient) used by the gridblock at the current time step. This allows the two models to capture the spatial and temporal changes in the flow system at the pore and field scales.

The objective of this work was to couple a first-principles network model with a reservoir simulator to capture the change in permeability, porosity, dispersion coefficient, and retention coefficient dictated by the structure of the porous medium at the pore-scale. In addition, a sensitivity analysis was carried out on the pore-scale model to determine the effects that particle size, number of particles injected, multiple particle species, and formation damage had on the determination of the continuum-scale parameters. Using boundary coupling, an injection scheme was developed where particles are injected into multiple networks in series to test the use of continuum-scale parameters at greater lengths and to validate the concurrently coupled model.

CHAPTER 2. BACKGROUND RESEARCH

Particle transport in porous media has been studied using experiments, analytical models, empirical models, and numerical simulation. Each of these approaches offer advantages and disadvantages. Experiments allow direct observation of the phenomenon; however it is hard to extrapolate results of experiments on a specific porous media to other specimens and this approach is generally limited to continuum-scale analysis. Analytical models can be applied to a broad spectrum of porous media and particle species. However analytical models may fail to include pore-scale heterogeneity and often require assumptions to be made about the pore structure. Empirical models, typically based on experimental or simulated data, can provide accurate solutions for a specific particle species and porous media but can be difficult to generalize to a broad variety of particle transport processes. Finally, numerical simulation can predict particle transport behavior quantitatively but involves assumptions and approximation and therefore must be validated by experimental results.

Pore-scale numerical simulation based on first principles rather than empirical relationships increases validity of the model. The 3-D network model offers a representation of pore-scale heterogeneity. In addition, 3-D network models use the fundamental equations that govern flow through porous media. Therefore, in this study, the particle plugging process is studied with a 3-D pore network model that predicts the capture of injected particles. A historical summary of pore network modeling is given, starting with the most basic petrophysical models.

2.1 Early Models of Porous Media

The first studies of fluid flow through porous media used the sphere-pack model (Hazen, 1892; Schlicter, 1899). Accurate descriptions of flow through this model were difficult to obtain due to the lack of computational methods. Kozeny developed an equation from the sphere pack, later modified by Carman, which relates permeability to porosity (Carman, 1937; Kozeny, 1927). The sphere pack model satisfies the interconnected nature of pores, but at the time of its development analysis of flow through it was not possible.

The bundle-of-tubes model represents the pore geometry as a bundle of capillary tubes and can be used to obtain equations for certain flow properties in porous media. The bundle of tubes model has successfully been used to correlate certain properties of porous media (porosity, permeability, capillary pressure). However, the model fails to accurately represent actual porous media. One example limitation is that real porous media are often more-or-less isotropic with respect to fluid flow while a bundle of tubes model is perfectly anisotropic (Fatt, 1956). The model is anisotropic because interconnectivity between adjacent tubes is not taken into account. The lack of interconnectedness makes it impossible to study the dispersion of solute because the particles will only travel down one path for the entire model. In addition, the model cannot capture the changes in velocity (acceleration or deceleration) that occurs in heterogeneous interconnected porous media. Although the bundle-of-tubes model provides equations to correlate flow properties of porous media, the major weakness of the model is the lack of interconnection between the tubes.

2.2 The Pore Network Model

A pore network model describes porous media as a collection of interconnected tubes and spheres. Pore network models have been used to study a number of fluid flow processes through many types of porous media. Early pore network models were 2-D and typically were solved using electric analogs. The results from 2-D models were qualitatively useful, but generally did not offer the ability to predict quantitative properties of porous media. Generating physically representative 3-D network models from simulated porous media or microtomographic images of real porous media has enabled their use for quantitative modeling of fluid and particle transport.

The first network model was developed by Fatt (1956) as a means to account for the interconnected nature of porous media. Fatt proposed that the two models used in the past, the sphere pack and the bundle of tubes, are too simple and the equations derived from them have failed to predict the observed properties of porous media. The agreement of these simplistic models with experimental observations is only achieved by inserting physically insignificant parameters (Fatt, 1956). For example the tortuosity parameter in the bundle of tubes model is not a physically determined parameter and is used to adjust the results of the model to fit experimental data.

Fatt's network model is a 2-D network of tubes, where each tube represents a pore space. The network of tubes is isotropic and the replacement of pore spaces with cylindrical tubes is a permissible assumption for well-consolidated sandstones (Fatt, 1956). Fatt explained that a 2-D model is analogous to a 3-D model. He justified his assumption by arguing that a 2-D model representing a small slice of a material sealed by two impermeable planes has the same properties as a cube of the same material (Fatt, 1956). For calculations, capillary pressure characteristics were evaluated by hand but the flow properties were determined using an analog computer formed by a network of electrical resistors. The analog computer solved a system of linear equations that were set up by applying a fluid-conservation equation around each node and assigning a flow conductivity to each bond (Fatt, 1956).

After Fatt's initial work, a number of network modeling advances were made in the following decades. Researchers improved pore-scale network modeling by creating image-based network models (Dullien, 1975), studying 2-D versus 3-D networks (Blunt and King, 1991; Chatzis and Dullien, 1977), and modeling phenomena such as multiphase flow and immiscible displacement (Blunt and King, 1991; Salter and Mohanty, 1982), reactive transport (Hoefner and Fogler, 1988), and particle transport (Rege and Fogler, 1987). Dullien (1975) used photomicrographic images to obtain the pore size distribution curve from a sample to develop an accurate model of permeability using a 3-D network of capillary tubes. Chatzis and Dullien (1977) studied the modeling of sandstones as 2-D and 3-D networks of tubes and concluded that 2-D models produce significantly different results than 3-D. In addition, they explained that development of realistic 3-D network models is dependent on the knowledge of the pore structure and topology of the porous medium. In their work, 3-D models only matched experimental results if a mathematical relationship between volume fraction and the diameter of pores was assumed. Mohanty and Salter (1982) were the first to include multiphase effects in a simple cubic network model and validated their model by reproducing experimental results. Hoefner and Fogler (1988) successfully modeled the dissolution of porous media and Rege and Fogler (1987) modeled

particle plugging in porous media. These are two examples of pore-scale processes that have significant macroscopic effects on fluid flow through porous media (due to permeability increase or reduction). Blunt and King (1991) studied immiscible displacements using network models and the upscaling of the two phase's relative permeabilities in 2-D and 3-D. Each of these works employed use of network models to solve realistic problems in porous media; however they required assumptions about the structure of the porous medium itself that limited their ability to physically represent actual porous media.

Network models have the ability to replicate the size, location, and interconnection of voids in real porous media. However, producing a physically representative network from real porous media is difficult. Most early network models used an assumed pore-size distribution to stochastically generate a network. This led many of the early network models to require calibration to fit experimental results because they were physical misrepresentations of the actual pore space. Two structural issues exist with these models: the networks don't preserve pore locations and the network parameters including interconnectivity and pore length are difficult to measure (Bryant et al., 1993). Stochastically generated network models are often limited by their lack of ability to accurately predict permeability and porosity and by the amount of structural tuning required to match experimental results (Bryant et al., 1993).

In 1993, Bryant et al. presented a new method for extracting a network model from a consolidated granular packing. Their work used a packing of uniform spheres with a known geometry and void space topology to produce physically representative network models. Their method employed a Delaunay tessellation to create a network model from the void space in the sphere packing. Bryant et al. compared the predicted porosity and permeability from the network model to the measured values from the sphere packing as a validation of the network's representation of the pore space. The method for extracting a physically representative network model increased interest in using network models as quantitatively predictive tools.

The work by Bryant et al. 1993 enabled the extraction of physically representative network models but was limited by its connection to a single granular packing. Work by Thompson and Fogler (1997) developed a general model for fluid and solute transport in an arbitrary disordered packed bed. Their work simulated disordered and heterogeneous packed beds and extracted physically representative network models from the beds. Like Bryant et al. 1993, the methodology was superior to previous network modeling techniques because it determined the disorder and heterogeneity in the porous medium rather than stochastically or randomly assigning physical property distributions onto the network (Thompson and Fogler, 1997). By improving network extraction methodology to allow the creation of networks from a variety of simulated porous media, Thompson and Fogler paved the path for the construction of image based network models.

Currently, pore network models are usually constructed from 3-D microtomography photographs of physical samples (such as core plugs) by identifying the void space and the constrictions. These models are a 3-D network of spherical nodes and cylindrical bonds that represent the computer identified pore spaces and constrictions. The ability to model 3-D flow through a network that is physically representative of a real rock enables the prediction of particle transport at the pore-scale.

2.3 Particle Deposition Network Models

Researchers have employed network models to simulate the particle deposition process for decades. Mechanical straining of particles, or large particles blocking pore throats, is the dominant mechanism for permeability reduction in porous media (Rege and Fogler, 1987). Additional capture mechanisms have been studied including surface attraction of charged particles and absorption of particles due to surface roughness. Network models are ideal for predicting particle deposition in porous media because they can track the path a particle takes through the model and determine if and where a particle is retained in the porous medium. The following section discusses a series of particle retention studies carried out using pore-scale network models.

The first study of particle transport in porous media was by Donaldson et al. (1977). The study included injection experiments and pore-scale modeling of fluid-particle suspension injections. The work hypothesized that the problem was a "random statistical process" and that particle retention is dependent on the path taken by the particle. The process was modeled in a bundle of capillary tubes, based on a pore size distribution, whereby the probability of a particle travelling into a capillary was proportional to the flow (Donaldson et al., 1977). If a particle is trapped in a capillary, the pressure is recalculated for that capillary to adjust the flowrate. Although the structure of the model was basic, the proposed particle path selection and trapping algorithm is the basis for more advanced particle straining simulations discussed in this section and used in this work.

Todd et al. (1984) attempted to model formation damage by injecting particles into a pore network model using a random walk particle path selection. In this method, each particle chooses its path through the network based on a random number. A number of particle capture mechanisms were considered including straining, random capture, settling, inertia, and hydrodynamic action (Todd et al., 1984). Although the model employed a variety of particle capture mechanisms, it failed to accurately capture the particle's path selection due to the use of the random walk. Rege and Fogler (1987) show that the random walk models for permeability reduction do not agree with experimental results quantitatively or qualitatively.

Rege and Fogler (1987) proposed a 2-D network model for tracking particles and determining whether or not a particle is trapped in the porous medium. Their model was created to study and depict formation damage (permeability reduction) caused by particle retention in porous media. The capture mechanism in the model is mechanical straining, which means if a particle is too large to travel through its selected flow path it is trapped in the porous medium. When large particles are injected into a porous medium and they are strained, the resulting formation damage is more severe than the damage caused by deposition of smaller particles due to other mechanisms (Rege and Fogler, 1987). This model was the first that considered simultaneous entry of suspended particles into the network to accurately represent a fluid-particle suspension injection. Each particle's path is tracked and governed by flow biased probability. The particle's path selection is stochastic in nature which means that a particle plugging experiment run twice under the same conditions could result in different number of entrapped particles. To make their model realistic, the concept of "flow biased probability" is used to dictate a particle's travel from node to node. The particles path selection depends on both probability and flow rate. Each exit

channel from a pore is assigned a probability. "The greater the flow rate, the greater the probability that the particle selects that exit channel" (Rege and Fogler, 1987). Their work observed that formation damage due to particle plugging can cause a drastic reduction on the permeability of porous media and was validated with experimental results. In addition, they showed that the use of flow rate biased probability produced a much higher level of agreement between the simulation and experiments than the random walk method previously employed by Todd et al. (1984).

Sharma and Yortsos (1987), proposed a pore network model for deep bed filtration. Their model includes particle trapping due to size exclusion and pore closure due to particle deposition on pore walls. To make the model analytically tractable, an effective media approximation (EMA) is used to describe the flow field (Sharma and Yortsos, 1987). They compared their results with a continuum model that used a filtration coefficient to determine how many particles were deposited in the porous medium. They proved that the general assumption that the filtration coefficient is constant for a given sample of porous media is only valid for pores of uniform size. They found that in general the filtration coefficient decreases with time and increases with distance along the filter. Most importantly, they found that the pore structure of the filter has significant impact on the filtration coefficient and permeability over time (Sharma and Yortsos, 1987).

A model proposed by Imdakm and Sahimi (1987) used a Monte Carlo simulation method to predict particle plugging in a statistically generated 2-D square pore network. The pressure is solved across the pore network and used to compute the flow rate through each pore throat. The flow rates are used to calculate the permeability across the network (Imdakm and Sahimi, 1987). The model uses the same particle path selection idea as Rege and Fogler (1986), where the particle is most likely to travel through the throat with the greatest flowrate. In 1991, they updated their model to include electrical charge and drag forces on particles. Depending on the sign of the electrical charge of a particle and the electrical charge of the surface, the particle is either repulsed or attracted to the surface. The fluid flow is slow enough to represent the flow field near the particles as linear shear flow which enables the use of exact expressions for drag force calculations (Sahimi and Imdakm, 1991). The exact path of the particle is numerically determined from the force and torque balances and if the path intersects the surface, the particle potentially attaches to the surface. The particle attachment is dictated by the roughness of the surface. Finally, they used their simulation method on a 3-D network model and were able to account for the effects of pore plugging, particle deposition, and macromolecular absorption onto the surface of the porous medium (Imdakm and Sahimi, 1991).

Meloy et al. (1991), used a 2-D network model to study the relationship between throat size distribution and particle plugging for single sized particle species. They examined the effect of four statistical distributions of throat sizes on the model: Rayleigh, Lognormal, Gauss, and Exponential. In their model, if a particle plugs a throat the throat conductivity goes to zero, which is equivalent to removing the throat from the network. They concluded that the difference in throat size distribution had no effect on the percentage of plugged throats and that the percentage of plugged throats is a function of the injected particle size (Meloy et al., 1991). In addition, they concluded that the percolation threshold is independent of the throat size distribution (Meloy et al., 1991).

Ochi and Vernoux (1999) used a 2-D network model to study the particle deposition process by considering three mechanisms: straining, particle interception, and particle diffusion. They considered particle release as a function of first order kinetic laws that relate the microscopic velocity of the fluid and a critical velocity. The simulations were run under constant pressure boundary conditions which caused the results to differ in comparison to experiments run under constant flow rate conditions (Ochi and Vernoux, 1999).

Siqueria et al. (2003) performed particle transport simulations on a 3-D network model generated from 2-D images of porous systems using geostatistical procedures. The key difference between their work and the previous authors is that their network is based on image analysis of real porous media and therefore yields realistic velocities at the pore-scale (Siqueira et al., 2003). Two main particle capture mechanisms are included: particle capture caused by interactions between the rock matrix and particles and straining of the particles (Siqueira et al., 2003). The paper explores the effects of pore throat shape and the pore interconnectivity. Additionally, the study highlights the potential to use macroscopic models to upscale the results to forecast damage in near wellbore systems.

Several important observations from these works are used to validate the particle plugging network model presented in this thesis. First, particle plugging of throats can cause significant permeability reduction of porous media (Rege and Fogler, 1987). Second, the retention coefficient generally decreases with time as the porous medium is plugged (Sharma and Yortsos, 1987). Third, the percentage of plugged throats (damage) is a function of the particle size (Meloy et al., 1991).

2.4 Coupling Network Models to Reservoir Simulators

In recent years efforts have been made to couple network and continuum-scale models. Three techniques have been used for the multiscale coupling: boundary coupling (Balhoff et al., 2008; Balhoff et al., 2007; Mehmani and Balhoff, 2014; Mehmani et al., 2012), sequential coupling (Blunt et al., 2002; Chen et al., 2010; Jackson et al., 2003; Lichtner and Kang, 2007; Rhodes et al., 2008; Sun et al., 2011; Tsakiroglou, 2012; White et al., 2006), and concurrent coupling (Battiato et al., 2011; Celia et al., 1993; Chu et al., 2012, 2013; Heiba et al., 1986; Sheng and Thompson, 2013; Van den Akker, 2010)

Like lab experiments, pore-scale models can be used to determine continuum-scale parameters that can be used in reservoir simulation studies. These parameters include absolute permeability, relative permeability to various fluid phases, dispersion coefficient, and particle retention coefficient. These parameters can be tabulated and used by a reservoir scale simulator to include pore-scale physics in the macroscopic model. However this tabulated approach offers no advantage over using experimentally determined reservoir properties. The real benefit of using pore-scale models to determine continuum-scale parameters is the ability to allow communication in both directions as a concurrently coupled model. The concurrently coupled approach enables the reservoir-scale model to provide conditions to the pore-scale model to determine certain systems parameters at the current time step. The three coupling techniques and their uses are discussed in detail in the following section.

2.4.1 Boundary Coupling

Pore-scale models can be linked to adjacent pore-scale or continuum-scale regions at their boundary. In boundary coupling, successful coupling at an interface requires matching the boundary conditions for the two-scales (Balhoff et al., 2007). Boundary coupling has been used for studying flow from a pore-scale model to a low permeability continuum-scale region (Balhoff et al., 2007), flow between multiple pore-scale models (Balhoff et al., 2008), and studying the spatial upscaling of reactive transport parameters determined using pore-scale models (Mehmani et al., 2012). Boundary coupling is useful for studying spatial upscaling because it allows pore-scale simulations to be run at greater lengths to validate the use of continuum-scale parameters obtained at the pore-scale.

In 2007, Balhoff et al. used boundary coupling to simulate flow through a packed bed of spheres into a homogenous low-permeability continuum region. The goal of the work was to couple a pore-scale network model with a continuum region and accurately predict flow between the two models using the correct boundary condition.(Balhoff et al., 2007). The boundary condition was determined with an iterative approach that matches the flowrates entering/exiting the pore-scale and continuum model. The coupled model was validated using a simple cubic sphere packing (no heterogeneity) and by checking agreement with the solution found by solving the same problem as a single continuum domain with distributed permeabilities (Balhoff et al., 2007). Running the coupled model with a random packing (heterogeneous) and comparing with a single continuum domain showed different pressure profiles across the length of the simulated region and proved that pore-scale heterogeneity can have a pronounced effect on the flowrate of the system. The model proved that coupling is necessary under certain circumstances because a standalone continuum model cannot include the pore-scale heterogeneity and a standalone pore-scale model cannot account for the added flow resistance of the adjacent continuum region. This method was rigorous but had limited practicality due to its computational inefficiency and limited applications.

Balhoff et al. (2008) presented a boundary coupling method using mortars to link two different models. In this work, two subdomains modeled different physics, implemented different finite difference or finite element meshes, and were solved independently. The boundary conditions at the interface are solved using mortar spaces. The mortar space is a 2-D finite-element discretization that projects pressure onto the subdomain (Balhoff et al., 2008). The projected pressure field is selected so that the change in flow rate across the boundary is zero. With this method a pore-scale model can be coupled to a different pore-scale model or to a continuum region. The mortars allow pressure and flow continuity between the two different models. This follow-up work by Balhoff et al. (2008) increased computational efficiency by using the mortar method and offers a greater number of applications than the previous boundary coupling study. The ability to connect two models implementing different solution methods (finite difference or finite element) and different domains (pore-scale or continuum-scale) is an important development for multi-scale modeling.

Mehmani et al. (2012) used mortar coupling to link multiple network models to run simulations at larger scales to increase the accuracy of upscaling approaches for the simulation of reactive CO_2 transport. Their work coupled networks with large variation in permeability and porosity to

initiate preferential pathways. Their simulations showed that the preferential pathways closed due to precipitation and eventually became disconnected. Mehmani and Balhoff (2014) proposed a hybrid mortar coupling method that can solve nonlinear flow problems using pore-to-pore and pore-to-continuum interfaces.

Boundary coupling offers the ability to inject fluid into multiple network models in series which allows one to impose greater heterogeneity at the pore-scale. More importantly, for this work boundary coupling allows you to use the same network in series to increase the length of the porous medium and study the validity of continuum-scale parameters obtained from a single network model at larger spatial scales. This will be discussed further at a later point in this document.

2.4.2 Sequential Coupling

In sequential coupling, the pore-scale and continuum-scale models are operated independently. The Continuum-scale parameters are determined using a pore-scale simulation and used in a reservoir simulator. This is analogous to using lab data in a reservoir simulation. This technique can require upscaling in both space and time.

Blunt et al. (2002) compared reservoir simulation results obtained using relative permeabilities predicted by a network model with results obtained using traditional empirical correlations. The work concluded that the predictive power of reservoir scale simulation can be improved by using network models to predict relative permeability. Other work focused on using Lattice Boltzmann methods (LBM) at the pore-scale coupled to continuum-scale simulators to study single phase flow (White et al., 2006), reactive flow (Lichtner and Kang, 2007), and permeability change due to colloid deposition (Chen et al., 2010).

Rhodes et al. (2008) examined the particle transport process at the pore, core, gridblock, and field scale. The study used a network model to predict how the Peclet number affected the dispersion coefficient. The dispersion coefficient was used to model particle transport at the core-scale. The transit time distribution for the injected particles was solved at the core and gridblock scales and used in the reservoir scale simulation. They found that field scale particle transport was affected by the pore-scale transport processes even when an extremely heterogeneous field scale reservoir description was used (Rhodes et al., 2008). They observed, that pore and core scale heterogeneity increased particle transit time and significantly delayed particle breakthrough time. The work concluded that it wrong to assume particle transport is only affected by reservoir scale geology (Rhodes et al., 2008).

The work of Rhodes et al. (2008) offers substantial proof that pore-scale heterogeneity has a pronounced effect on particle transport at the reservoir scale. A drawback to the sequential coupling method is that it can’t predict the changes in particle retention and dispersion occurring in time. Allowing the pore-scale simulator and reservoir simulator to march forward in time together enables the prediction of changing continuum-scale parameters as the porous medium is damaged. This procedure will be discussed in the following section: Concurrent Coupling.

2.4.3 Concurrent Coupling

Sequential coupling offers the potential to replace core flooding experiments with numerical simulations but does not allow the models to march forward together in time. Concurrent coupling allows the models to communicate back and forth at each time step which is beneficial for the study of transient flow systems. Only a few concurrent network models have been successfully executed to date. Celia et al. (1993) and Van den Akker (2010) both proposed concurrent simulation strategies, but they were not implemented at the time due to computational limitations. Battiato et al. (2011) used concurrent coupling to place network models in grid block locations where flow violates assumptions made by the continuum-scale model. Chu et al. (2012) created a single phase concurrently coupled model to simulate non-Darcy flow. Sheng and Thompson (2012) used a concurrently coupled model to include the dynamic nature of relative permeability captured by pore-scale information to improve continuum-scale simulation of immiscible displacements.

Sheng and Thompson (2012) embedded a multiphase flow pore-scale network model into continuum-scale gridblocks of a reservoir simulator. The models communicated back and forth. The reservoir simulator supplied the fractional flow at the boundary and the network model passed back the time dependent relative permeabilities. To demonstrate the power of the concurrently coupled simulator, the study examined the rate dependent behavior of relative permeability. The author pointed out that changes in injection rate affected the capillary number which can have an impact on relative permeability (Sheng and Thompson, 2013). Variable-rate injection experiments were carried out in 1-D with 3 network models embedded in 3 of the 100 continuum gridblocks. The gridblocks with the network models showed a significant difference in phase saturation. The study concluded that "the ability for a reservoir-scale model to obtain continuum parameters directly from a first principles model enables it to respond to any number of phenomena that are not captured by empirical relationships or tabulated parameters" (Sheng and Thompson, 2013).

The work of Sheng and Thompson (2012) is similar to the work presented in this thesis in that the network models are embedded into continuum-scale gridblocks and the two systems march forward in time together. The purpose of their work was to show that continuum-scale parameters often are time dependent which is an important observation from this work as well. This thesis shows that continuum-scale particle transport parameters are not only time dependent, but also change with respect to particle size distribution, suspension concentration, and the porous medium itself. The following sections will discuss the development of a concurrently coupled particle plugging simulator and the prediction of time dependent continuum-scale properties that are passed to the reservoir simulator.

CHAPTER 3. MODEL DEVELOPMENT

The proposed multiscale particle plugging model couples a pore network model with a reservoir scale model (the latter using a streamline simulation approach). The reservoir model provides the inlet velocity, the particle species diameters, and the particle species concentrations to the pore network model. The pore network model computes the dispersion coefficient, particle retention coefficient, reduced permeability, and the reduced porosity caused by particle plugging and passes those parameters back to the reservoir scale model. The two simulators are concurrently coupled and march forward in time together. The aim of the coupled model is to simulate the effects of particle migration in a petroleum reservoir. Additionally, the coupling technique used lays the foundation for coupling streamline simulators with more sophisticated pore-scale models that include other particle absorption mechanisms. Such models could be used for modeling nanoparticle transport in petroleum reservoirs. The following sections will discuss the pore-scale particle plugging model, determination of the retention coefficient, coupling multiple network models, and coupling the network model with the reservoir scale model.

3.1 The Pore-Scale Model

The pore-scale particle transport network model only considers mechanical straining of the particles as they travel through the porous medium. The particles flow through a 3-D pore network that is generated from simulated porous media or microtomography images of real porous media. Similarly to previous work, the particle path selection is stochastic but a particle is most likely to select the path with the largest flowrate. The permeability and porosity reduction is calculated each time a particle is trapped in the porous medium. After injection is complete, an effluent particle concentration curve is produced from the simulation results. The following sections explain the network model, solving the pressure field in the network, and the particle plugging simulation.

3.1.1 The Network Model

Table 1: Summary of Berea Sandstone network model parameters.

Berea Sandstone Network Model Parameters	
Dimensions:	0.3502 x 0.3502 x 0.227 cm^3
Number of Pores:	30,042
Number of Throats:	135,045
Porosity	15.24%
Permeability	611 mD

In this project, the 3-D network model was produced from microtomographic images of a Berea Sandstone core. The network model represents a 0.3502 x 0.3502 x 0.2270 cm^3 portion of the core and consists of 31,400 pores and 137,215 throats. An additional processing step is required for the model; removal of the boundary throats and dead pores. The boundary throats must be removed because we are assuming no-flow boundary conditions on the faces that are not the inlet

or outlet. The dead pores must be removed because they represent voids that cannot be reached by fluid flow, which can cause singularities in the matrix solution. After removal of the dead pores and boundary throats, the network model consists of 30,042 pores and 135,045 throats. The properties of the Berea Sandstone network model are summarized in table 1 below.

The porosity, calculated by summing the volume of the pores and dividing by the total volume of the sample, is 15.24%. The permeability, calculated by simulating flow and applying Darcy's law, is 611 mD. This is in good agreement with experimental permeabilities of the block that the tomography core was obtained from.

3.1.2 Solving the Pressure Field

The pressure field of the network model is obtained by solving a system of linear equations representing the conservation of mass at each pore. The fundamental equations for solving the pressure field of the network are described in this section. For single phase fluids, the conservation equation for pore *i* is (Balhoff et al., 2007):

$$\sum_{j} q_{ij} = 0 \tag{1}$$

In this equation q_{ij} is the volumetric flow rate through a throat that connects pore *i* to a neighboring pore *j*. The flowrate is a function of the unknown pore pressures (p_i) the fluid conductivity in the throat (g_{ij}), and the fluid viscosity (μ) as shown in Equation 2.

$$\sum_{j} q_{ij} = 0 \; = \; \sum_{j} [(p_j - p_i)\frac{g_{i,j}}{\mu}] \tag{2}$$

The fluid conductivity is the ratio of volumetric flow rate to pressure drop across a pore throat and is independent of fluid viscosity. Equation 2 is formulated into a system of equations to solve for the pressure in each pore. This conservation model is further modified to represent a constant rate (Q) injection by adding a constraint to the matrix that represents the sum over all inlet pores (Thompson and Fogler, 1997):

$$Q = \; \sum_{j} [(p_{inlet} - p_i)\frac{g_{i,j}}{\mu}] \tag{3}$$

The system of linear equations is solved using one of a variety of iterative techniques good for solving large and sparse matrices, for example the Gauss Seidel method.

3.2 The Particle Plugging Simulator

The pore-scale particle plugging simulator tracks particles as they are injected into a pore network and determines if and where they are retained. The simulator only considers one

trapping mechanism: size exclusion. Size exclusion or physical straining of particles occurs when the particle diameter is larger than the throat diameter that it is travelling through. If a particle is trapped, it reduces the permeability and porosity of the network model. A flow chart of the particle plugging simulator is shown in Figure 27 in the Appendix and will be discussed in detail in the following sections.

3.2.1 Initializing the Model

All of the parameters describing the pore network are stored in one data file. The data include the number of pores, number of throats, volume of pores, radius of throats, hydraulic conductance of the throats, interconnectivity of the pores and throats, and locations of the pores. The pressure field for the initial (undamaged) model is solved first using the method outlined in the previous section. The initial porosity is determined by summing the volume of each pore and dividing that sum by the bulk volume of the sample. The permeability in the direction of injection is calculated using Darcy's law as shown below.

$$\mathrm{k} = -\frac{\mathrm{Q\mu L}}{\mathrm{A\Delta P}} \tag{4}$$

Here Q is the total inlet flowrate into the model, μ is the viscosity of the fluid, L is the length in the direction of injection, A is the cross sectional area of the injection face, and ΔP is the pressure difference between the boundary outlet and inlet. The total inlet flow rate is determined by finding all of the inlet pores and throats at the injection face and summing their respective flowrates. Each inlet pore or inlet throat flow rate is based on the hydraulic conductivity of the throat and the pressure drop across the throat. After the determination of the initial parameters of the model, the particle injection simulation begins.

3.2.2 Particle Injection Scheme

Generally we are modeling processes where injected particles flow through the porous medium simultaneously. However, the simulator tracks the path and travel time of the particles individually. When the simulation begins, the first particle is injected and tracked. If that particle is trapped in the porous medium, the pressure field is recalculated and the next injected particle is tracked. If the particle exits the porous medium, the next injected particle is tracked using the previous pressure field because the porous medium has not changed. The details of the particle injection and tracking are discussed in this section.

A particle is injected into either an inlet throat or inlet pore. The injection point is selected by generating a random number and choosing one of the inlet pores or throats. The inlet is chosen based on its fractional flow. The cumulative inlet flowrate is determined for the inlet face and used to calculate a fractional inlet flow rate for each inlet throat and pore. The greater the fractional flow rate into a throat or pore, the higher the probability that a particle chooses that entrance point. Once the particle has entered the porous medium, the path selection of the particle is dictated by the same flow rate bias concept used by Rege and Fogler (1986) and

originally proposed by Donaldson (1977). When a particle enters a pore, a random number is generated (between 0 and 1) and if that number falls between the number range allocated to a certain throat then that path is selected. The number range is allocated to a throat based on the probability that a particle will travel into that throat. The probability of a particle travelling into a throat is the fractional flow into the throat. Consider Figure 1.

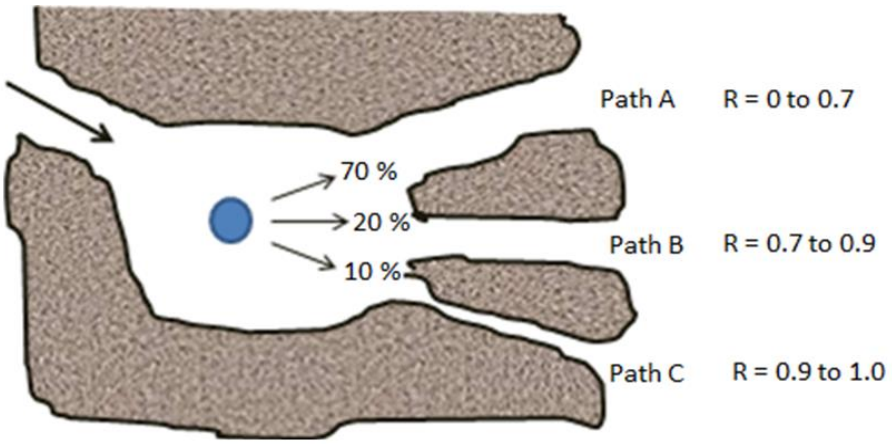

Figure 1 : A particle's path selection based on flow rate biased probability (Rege and Fogler, 1987).

A particle travels into a pore with three possible exit throats. Path A has a flowrate that represents 70% of the total flowrate out of the pore, Path B 20% of the total flowrate, and Path C 10% of the total flowrate. In this case if the random number, R, falls between 0 and 0.7, then the particle will travel through path A. If the random number falls between 0.7 and 0.9, the particle will travel through path B. Therefore a particle is most likely to select the path with the greatest flowrate, but a particle still has the chance of taking the more constricted path. This method of particle path selection includes not only the physics of particle transport, but also its stochastic nature.

If a particle is too large to travel through the selected path it is trapped in the throat. This particle trapping mechanism known as physical straining or size exclusion is the only particle deposition mechanism included in this model. If a particle is trapped, the surface area of the throat is increased by the surface area of the trapped particle and the cross sectional area of the throat is reduced by the cross sectional area of the trapped particle. This reduces the effective radius and the hydraulic conductivity of the throat. Reducing the hydraulic conductivity of the throat will decrease the likelihood of a particle selecting that path in the future and will decrease the overall permeability of the network. The pore throats do not actually represent volume in the model only the restriction of flow from one pore to another. Therefore, when a particle is trapped, the pore volume of the pore that the particle was travelling from is reduced by the volume of the particle. The reduction of pore volume reduces the overall porosity of the network. Finally, the relative spatial location of the trapped particle is computed from the pore location to visualize the distribution of trapped particles in the network during post processing.

If a particle passes through the porous medium, the particle's transit time is recorded. As the particle travels through the network, the transit time is updated by adding the ratio of pore volume of the next pore to the flow rate out of the previous pore. This is the amount of time it takes for the fluid transporting the particle to flow from one pore to the next. When the particle exits, the transit time is the amount of time that it took the particle to travel through the network from inlet to outlet.

If the particle exits the porous medium, the previous pressure field solution can be used for the next particle. However if a particle plugs the porous medium, the pressure field must be recalculated for the entire network to account for the reduction of hydraulic conductance in the throat where the particle was trapped. Once all of the particles have been injected and tracked the simulation routine is finished.

3.2.3 Effluent Curve from Particle Plugging Simulation

Examination of the effluent concentration curve is a common method for analyzing particle suspension injection experiments or simulations. An effluent concentration curve shows the change in the concentration of the injected particle suspension with respect to pore volumes of fluid injected. The shape of the effluent concentration curve is influenced by the dispersion and retention of injected particles in the porous medium. This section explains how an effluent concentration curve is generated from the particle plugging simulation data.

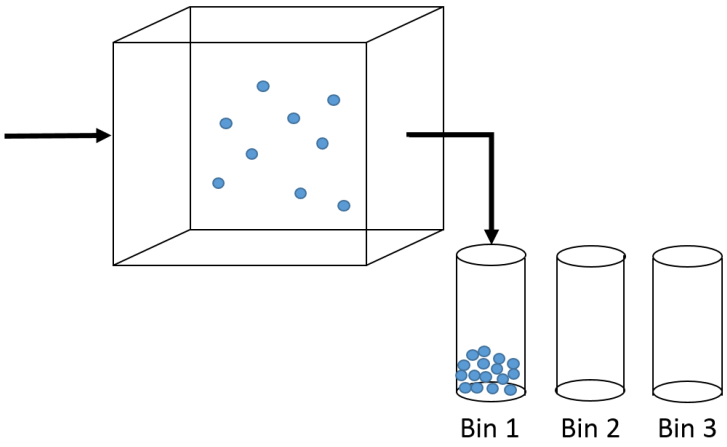

Figure 2: A depiction of the particle binning process used to generate the effluent concentration curve from the pore-scale simulation results.

The effluent curve is created using the binning concept. Figure 2 above is a schematic of the particle binning process. Imagine a core flooding experiment where a particle suspension is being injected into a permeable sandstone core. At the outlet the particle suspension will eventually break through. To understand how the concentration is changing at the outlet with respect to time, a lab assistant holds a test tube (bin) at the outlet for a certain amount of time and then changes test tubes. This process would be continued until all of the fluid has left the core. Each test tube represents a data point in time with an expected number of particles. To determine

the change in concentration at each data point, the number of particles in each test tube is divided by the expected number of particles. This fraction is the same as the change in concentration, C/C_0, and can be plotted against pore volumes injected or time to make an effluent concentration curve.

It is simple to apply the particle binning concept to the particle plugging data. Each particle has a release time and transit time associated with it. Therefore the point in time at which a particle leaves the porous medium during an experiment is the sum of the particle's release and transit times. An array of bins is created to store the particles exiting the porous medium. Each bin represents a fixed volume of fluid and a period of time during the simulation. For example for a bin size of 0.1 pore volumes, bins 1, 2, and 3 would represent 0.1, 0.2, and 0.3 pore volumes injected respectively. The expected number of particles for a bin is computed by multiplying the bin's volume by the inlet concentration. If the time a particle leaves is during the time period represented by a particular bin, then that particle is stored in that bin. Each bin represents a relative concentration data point on the effluent concentration curve.

3.3 Determination of the Retention Coefficient

The key continuum-scale parameter for the pore-scale to reservoir scale coupling is the retention coefficient for each particle species travelling through the pore space. This parameter is used in the streamline reservoir simulator to quantify how many particles of each species will be deposited in the reservoir rock. The determination of the retention coefficient requires the application of classical colloid filtration theory.

3.3.1 Classical Colloid Filtration Theory Model

The advection-dispersion equation predicts the change in colloid concentration in space and time for a fluid suspension injected into a homogenous granular porous medium (Golzar et al., 2014):

$$\frac{\partial \mathrm{C}}{\partial \mathrm{t}} = \mathrm{D}\frac{\partial^2 \mathrm{C}}{\partial^2 \mathrm{x}} - \mathrm{U}\frac{\partial \mathrm{C}}{\partial \mathrm{t}} \tag{5}$$

This equation applies to the change in concentration across a porous medium in 1-D. This basic form of the advection dispersion-equation only considers the change in concentration due to longitudinal dispersion (D) and the interstitial velocity (U). The equation can be modified to include the deposition, attachment, and detachment of particles in the porous medium. When particles are removed from the liquid phase due to straining or surface absorption, the general advection dispersion equation becomes (Golzar et al., 2014):

$$\frac{\partial \mathrm{C}}{\partial \mathrm{t}} + \frac{\rho_\mathrm{b}}{\varphi}\frac{\partial \mathrm{C}}{\partial \mathrm{x}} = \mathrm{D}\frac{\partial^2 \mathrm{C}}{\partial^2 \mathrm{x}} - \mathrm{U}\frac{\partial \mathrm{C}}{\partial \mathrm{t}} \tag{6}$$

In this work, the detachment or release of particles is not considered. The only mechanism considered in this project is the mechanical straining of particles. In classical colloid filtration

theory (CFT), particles can only be retained not released. Therefore in CFT the following equation applies (Golzar et al., 2014):

$$\frac{\rho_b}{\varphi}\frac{\partial C}{\partial x} = k_r C \tag{7}$$

Based on the CFT the following equation governs the transport and fate of a particle suspension in a one dimensional, homogenous, porous medium (Golzar et al., 2014):

$$\frac{\partial C}{\partial t} = D\frac{\partial^2 C}{\partial^2 x} - U\frac{\partial C}{\partial t} - k_r C \tag{8}$$

Where *C* is the concentration of the particle suspension and k_r is the retention coefficient. This equation can be solved numerically using properly chosen boundary conditions.

A numerical simulation of Equation 8 was developed to determine the change in concentration of a particle species with respect to space in time during injection of a particle suspension. This continuum-scale numerical simulation code was developed using a finite difference discretization of Equation 8 based on the work of Golzar et al. (2014).The variables of the transport equation are nondimensionalized as follows:

$$\begin{aligned} D^* &= \frac{D}{LU}, \qquad k_r^* = \frac{k_r L}{U} \\ U^* &= \frac{U}{U_0}, \qquad C^* = \frac{C}{C_0} \\ x^* &= \frac{x}{L}, \qquad t^* = \frac{tU}{L} \end{aligned} \tag{9}$$

Where *L* is the length of the porous medium parallel to injection, *x* is the location along the length of the porous medium, *t* is the time from the beginning of injection, and C_0 is the initial concentration at the injection face. Using the dimensionless variables, Equation 4 can be rewritten as follows.

$$\frac{\partial C^*}{\partial t} = D^*\frac{\partial^2 C^*}{\partial^2 x^*} - U^*\frac{\partial C^*}{\partial t^*} - k_r^* C^* \tag{10}$$

Equation 10 is discretized into a finite difference formula using the Laasonen method which is unconditionally stable (Golzar et al., 2014). The discretized equation is show below.

$$\left[-\frac{D^*\Delta t^*}{\Delta x^{*2}} - \frac{U^*\Delta t^*}{2\Delta x^*}\right] C_{i-1}^{*n+1} + \left[1 + \frac{2D^*\Delta t^*}{\Delta x^{*2}} + k_r^*\Delta t^*\right] C_i^{*n+1} + \left[-\frac{D^*\Delta t^*}{\Delta x^{*2}} + \frac{U^*\Delta t^*}{2\Delta x^*}\right] C_{i+1}^{*n+1} = C_i^{*n} \tag{11}$$

To solve Equation 11 the proper boundary conditions must be implemented into the solution algorithm. A Dirchlet (constant concentration) boundary condition is used at the inlet and a

Neumann (no flux) boundary condition is used at the outlet. At the inlet, the concentration remains constant throughout the injection process. At the outlet, it is assumed that the concentration is the same as the concentration at the final spatial step of the simulation.

The 1-D simulator was developed to work for any number of spatial and time steps and solves the system of finite difference equations at each time step. Each spatial step has a finite difference equation, therefore the number of equations is equal to the number of spatial steps. The coefficients of the system of equations form a tridiagonal matrix system. The Dirchlet boundary condition is included in the coefficient matrix, A, and the solution vector, b. The Neumann boundary condition is only included in the solution vector. The coefficient matrix and solution vector are shown below for the case of 3 spatial steps.

$$A = \begin{bmatrix} 1 + \frac{3D^*\Delta t^*}{\Delta x^{*2}} + k_r^*\Delta t^* + \frac{U^*\Delta t^*}{2\Delta x^*} & -\frac{D^*\Delta t^*}{\Delta x^{*2}} + \frac{U^*\Delta t^*}{2\Delta x^*} & 0 \\ -\frac{D^*\Delta t^*}{\Delta x^{*2}} - \frac{U^*\Delta t^*}{2\Delta x^*} & 1 + \frac{2D^*\Delta t^*}{\Delta x^{*2}} + k_r^*\Delta t^* & -\frac{D^*\Delta t^*}{\Delta x^{*2}} + \frac{U^*\Delta t^*}{2\Delta x^*} \\ 0 & -\frac{D^*\Delta t^*}{\Delta x^{*2}} - \frac{U^*\Delta t^*}{2\Delta x^*} & 1 + \frac{D^*\Delta t^*}{\Delta x^{*2}} + k_r^*\Delta t^* + \frac{U^*\Delta t^*}{2\Delta x^*} \end{bmatrix} \quad (12)$$

$$b = \begin{bmatrix} C_1^{*n} + \frac{2D^*\Delta t^*}{\Delta x^{*2}} + \frac{U^*\Delta t^*}{\Delta x^*} \\ C_2^{*n} \\ C_3^{*n} \end{bmatrix} \quad (13)$$

The coefficient matrix and solution vector are used to implicitly solve for the spatial distribution of concentration at the next time step as shown below.

$$[A][C^{*n+1}] = [b] \quad (14)$$

Equation 14 is solved using the well-known Tridiagonal Matrix Algorithm (TDMA). The TDMA is a fast and memory-efficient solver that is easy to implement.

The 1-D simulator produces an effluent concentration curve of an injected particle suspension. As discussed previously, an effluent concentration curve is a plot of the relative concentration, C/C_0, versus the pore volumes of fluid injected. In the CFT model, the shape of the effluent curve is controlled by two continuum parameters: the retention coefficient and the hydrodynamic dispersion coefficient. The effects of the dispersion and retention coefficient are discussed in the following section.

3.3.2 Effect of the Dispersion Coefficient

The dispersion coefficient in the CFT model accounts for the variety of paths and speeds that particles follow to reach the outlet of the porous medium. Figure 3 shows three effluent curves generated by the CFT simulator for three different dispersion coefficients.

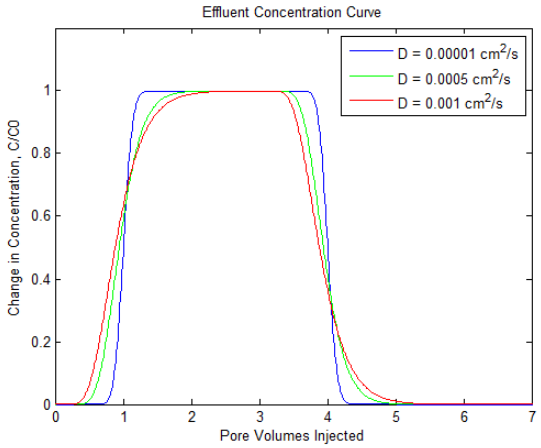

Figure 3: Effluent concentration curves generated by the CFT simulator for three different hydrodynamic dispersion coefficients.

Increasing the dispersion coefficient decreases the slope on the foot and tail of the concentration curve, indicating a more gradual change in concentration over time (in the effluent curve for instance). In addition, increasing the dispersion coefficient causes earlier breakthrough time for the particle suspension. A zero dispersion coefficient yields C/C_0 equal to 1 at breakthrough time and the curve becomes a shock front.

3.3.3 Effect of the Retention Coefficient

The retention coefficient in the CFT model accounts for the deposition of particles in the porous medium due to plugging or surface absorption. Figure 4 below shows three effluent curves generated by the CFT simulator for three different retention coefficients.

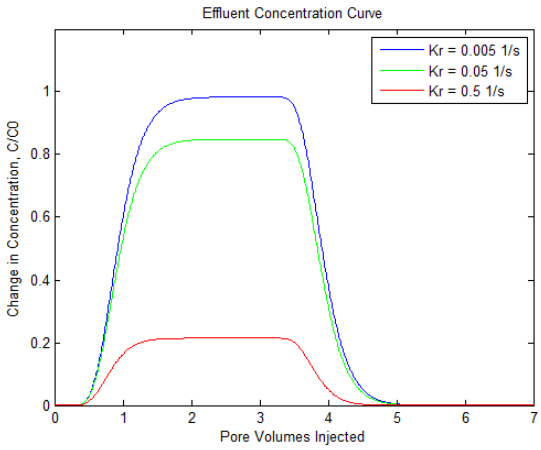

Figure 4: Effluent concentration curves generated by the CFT simulator for three different retention coefficients.

Increasing the retention coefficient decreases the crest of the effluent concentration curve (C/C_0 at the outlet decreases). A zero retention coefficient yields a peak C/C_0 equal to 1.

3.3.4 Fitting the CFT Model to the Pore-Scale Data

In particle injection experiments, each particle species will yield a unique dispersion and retention coefficient. The dispersion and retention coefficient are not only a function of the porous medium structure, but also the particle species properties. To determine the dispersion and retention coefficient for a given particle species, the CFT model is fit to the effluent concentration results from the pore network model. The fitting is done by adjusting the dispersion and retention coefficient until the sum of the squared errors between the CFT data and the pore-scale data is minimized. The dispersion and retention coefficient that yield the best fit are the continuum-scale parameters reported for that particle species.

Three approaches are used to determine the dispersion and retention coefficient that yield fits to the pore-scale data. In the first approach, it is assumed that the dispersion coefficient is independent of particle size and that it can be determined accurately by injecting a particle size where all of the particles pass through the porous medium. This effluent curve shows zero retention and therefore the retention coefficient is zero. After determining the dispersion coefficient the particle species of interest is injected and the retention coefficient is determined. To determine the best fit, the sum of the squared errors of the data points on the pore-scale and CFT effluent data is calculated. The dispersion or retention coefficient is adjusted in small increments from a very small value to a large value, and the dispersion or retention coefficient yielding the minimum sum of squared error is the respective continuum-scale parameter. This method is referred to as the linear step method.

Using small enough increments, the linear step method produced accurate results for both the dispersion and deposition coefficient. However this accuracy required sacrificing speed and the use of the assumption that the dispersion coefficient remains constant through the particle plugging process (which is invalid). For reasonable accuracy, determination of the coefficient required solving the CFT model approximately 10,000 times and selecting the best fitting result. This method is inefficient computationally and used a physically incorrect assumption.

Similar to the first approach, the second approach first finds the dispersion coefficient by fitting the CFT model to pore-scale data where no particles plugged (zero retention) and then finding the retention coefficient using the dispersion coefficient previously calculated. The second approach approximates the error profile as a parabola. Where the best fit is at the minimum of the parabola. In this method, three guesses for the coefficient were made. Two of the guesses, low and high values, bracket the coefficient and one of the guesses is in between the two brackets. The sum of the squared error is computed for each guess and a parabola is computed from the three two dimensional data points (coefficient, error). The minimum of this calculated parabola is the new middle guess and either the left or right bracket is replaced with the previous middle guess. This allows the solution algorithm to march towards the minimum error.

This bracketing method solves for the coefficients much faster than the linear step method however it has a key shortcoming. The bracket has to be properly chosen so that you are close enough to the solution that the error profile is approximately parabolic. Therefore this method is only useful if you have run tests on the porous medium and particle species of interest and can bracket the coefficient within +/- 100% of the solution. For this reason, this bracketing method is simply not a good option for determining the retention coefficient because in most cases the root is not properly bracketed. In addition, it also uses the invalid assumption that the dispersion coefficient remains constant throughout the plugging process.

The third method, the Nelder-Mead Simplex algorithm, solves for the dispersion and retention coefficient simultaneously and is fast and memory efficient. The method improves computation time in two ways. First, it removes the need to run two sets of particle injection scenarios, one where all the particles pass (finding D), and one where the actual particle species of interest are injected (finding k_r). Second, it solves the CFT model far fewer times than the linear step method which significantly reduces computation time and memory usage.

The Nelder-Mead Simplex algorithm discussed in this section was taken from Numerical Methods Using Matlab (4th Edition) by Matthews and Kurtis (2004).The Simplex algorithm uses three guesses of each coefficient to generate an equilateral triangle of data points in a 2-D plane with dimensions D and k_r. To find the D and k_r combination that yields the minimum error, the triangle undergoes the following operations: reflection, expansion, contraction, and shrinking. The four operations are shown in Figure 5 below.

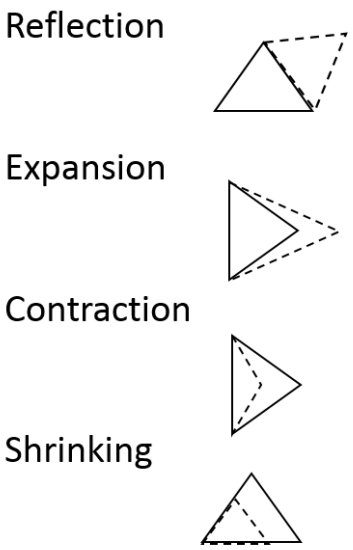

Figure 5: Four operations of the Nelder-Mead Simplex Algorithm, reflection, expansion, contraction, and shrinking of the triangle.

Considering the initial equilateral triangle and the error associated with each guess, there is a best (B), good (G), and worst (W) guess. The midpoint (M) is calculated between the best and good guess as follows (Mathews and Fink, 2004):

$$\mathrm{M} = \frac{\mathrm{B} + \mathrm{G}}{2} \tag{15}$$

The primary operation, the reflection is carried out by replacing the *W* point with a reflection point (*R*). From *M* and *W*, *R* can be calculated (Mathews and Fink, 2004):

$$\mathrm{R} = 2\mathrm{M} - \mathrm{W} \tag{16}$$

If the error associated with *R* is smaller than the error associated with point *W*, then the triangle has moved in the right direction. It is possible that the minimum error is just slightly further than point *R*. We can extend the triangle past point *R* to an expansion point (*E*). From *M* and *R*, *E* can be calculated (Mathews and Fink, 2004):

$$\mathrm{E} = 2\mathrm{R} - \mathrm{M} \tag{17}$$

If the error is smaller at *E* than at *R*, then the new vertex is *E*. If the error associated with *R* is equal to the error associated with *W*, the triangle is contracted rather than expanded. The contraction point (*C*) is found by calculating two new midpoints, *C1* and *C2* (Mathews and Fink, 2004). *C1* is the midpoint between *W* and *M* and *C2* is the midpoint between *R* and *M*. *C* is chosen as *C1* or *C2* based on which point has the smaller error.

Finally, if *C* is not less than *W*, the points *G* and *W* must be moved towards *B*, thus shrinking the entire shape of the triangle. To shrink the triangle, *G* is replaced with *M* and *W* is replaced with the midpoint between *B* and *W*. The four operations were coded into the software using the following flowchart shown in Figure 6:

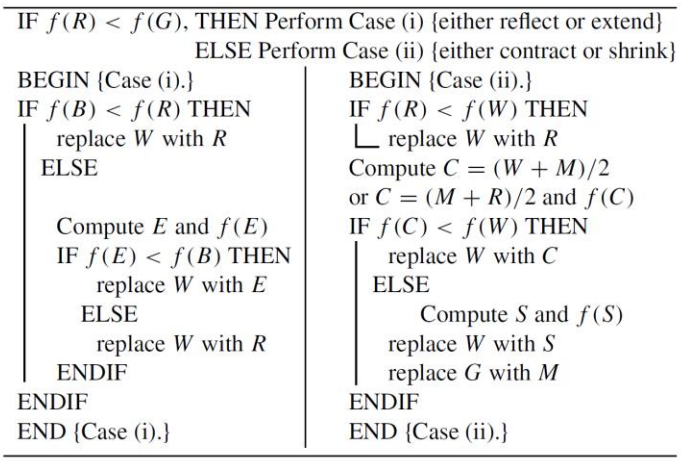

Figure 6: Flowchart of Nelder-Mead Simplex algorithm used for finding the dispersion and retention coefficient simultaneously (Mathews and Fink, 2004).

Using the simplex algorithm, the dispersion and retention coefficient for each injected particle species is determined.

The simplex algorithm has one weakness: it finds the local minimum of a function. In the case of fitting the CFT model to the particle plugging simulator effluent data, the simplex algorithm finds the D and k_r that produces the minimum error. The error profiles that are a function of D and k_r were generated to check that there is only an absolute minimum rather than several local minima. These error profiles were generated for a particle injection simulation where 10 micron particles were injected using the particle plugging simulator to produce an effluent curve. The error profiles are shown in Figure 7. Both error profiles show that there is an absolute minimum and no local minima. This ensures that the simplex algorithm is finding the best possible fit for the two data sets.

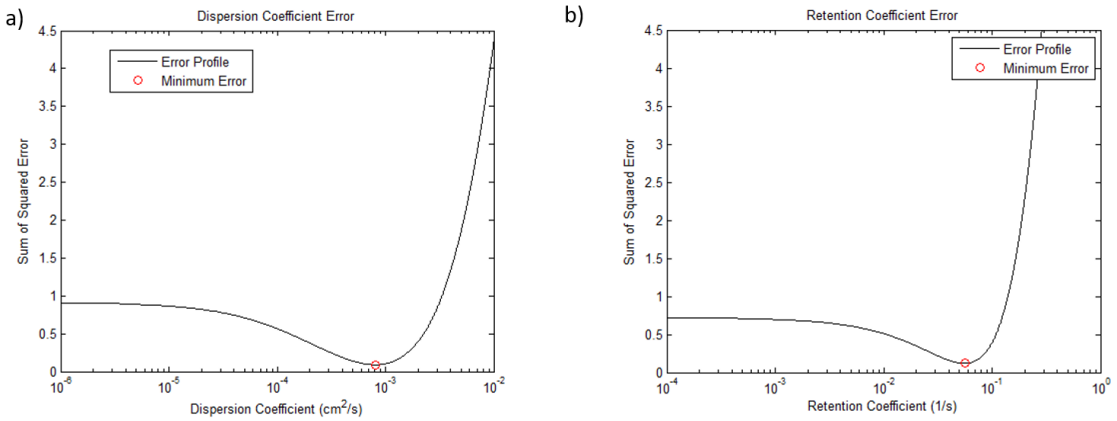

Figure 7: The error between the CFT and particle plugging simulator effluent curves as a function of (a) dispersion coefficient and (b) retention coefficient. Both error profiles show there is one absolute minimum in the error function.

3.4 Injecting into Multiple Network Models in Series

A network model may be limited in length by the size of the porous medium sample image. To simulate a longer sample of the same porous medium, the particle plugging simulator was adapted to inject through a collection of network models in series. Multiple network models are coupled at the boundary. This enables the user to run simulations through a core sample N times greater in length, where N is the total number of network models in series. This section discusses how the code was modified to allow injection of particles through multiple identical network models connected in series using boundary coupling. This model is referred to as the boundary coupled model in the rest of this thesis.

The key to injecting particles through multiple networks in series is keeping track of the time a particle exits a network model. An array containing every particle diameter and its initial release time is generated prior to the simulation. This array is read into the particle plugging simulator and dictates when each injected particle is released into the porous medium. If a particle passes all the way through, the sum of the particle release and transit time and the particle diameter are stored in a new array. This array of particles passing through the network model is the particle array used by the next network model in series. By updating the release times and total number

of particles injected at each network model in series, you end up with a final array of the particles that have passed through the entire network and their total transit time. The binning concept, previously explained, can be used to generate an effluent concentration curve for the multiple networks in series model.

The retention and dispersion coefficients are determined at each boundary of the coupled networks. This allows one to study how the dispersion and retention coefficient change as length of the sample is increased, which offers insight on the upscaling of the two parameters. The two coefficients are determined the same way they are determined for a single network, using the simplex algorithm to fit the CFT model to the pore-scale effluent data.

Injecting through multiple network models is useful for studying particle injection across greater lengths, studying the use of the retention and dispersion coefficients at greater length, and most importantly for validating the concurrently coupled model. These three topics will be covered in the *Results* section.

3.5 Coupling the Pore-Scale and Reservoir Simulators

The pore-scale particle plugging model was concurrently coupled with a reservoir simulator. The reservoir simulator predicts the change in concentration of particle suspension across gridblock using an advection-dispersion model. A pore-scale network model can be embedded in one or more of the reservoir model grid blocks and provides the reservoir simulator parameters for solving the advection-dispersion equation. The reservoir simulator updates the boundary conditions of the pore-scale network model at each time step to reflect the current flow conditions. The coupling process is discussed below in detail.

The reservoir simulator is a streamline model; therefore the spatial distribution of fluid velocity is predicted at each time step. The reservoir simulator passes the inlet velocity and particle species concentrations to the pore-scale network model. For the simulations shown here, particle species is dictated by the size (diameter) of the particle, and each particle species has a concentration. The inlet velocity and concentration are the boundary conditions for the constant flowrate particle injection simulation carried out with the pore-scale network model. In addition, the reservoir simulator tells the pore-scale network model the length of time to simulate (one time step of the reservoir model).

The pore-scale simulator is run using the inlet velocity, particle species concentrations, and time step dictated by the reservoir simulator. The change in porosity and permeability of the network are calculated. The pore-scale simulation results are fit with the continuum-scale CFT model as discussed in the previous section, and the dispersion and retention coefficient are determined. Finally, the pore-scale simulator passes the porosity, permeability, and retention coefficient to the reservoir simulator. The altered network is saved for each embedded gridblock so that the changes to the structure will be reflected during the next time step.

The reservoir simulator uses the retention coefficient from the embedded pore-scale simulator to predict the change in concentration of the particle suspension across the predicted streamline.

This process can be repeated over many time steps and the two simulators march forward in time together. The concurrent coupling captures the transient behavior of the particle plugging process and allows the model to adapt to an unlimited number of particle injection scenarios without relying on tabulated or empirical data.

CHAPTER 4. RESULTS

Particle plugging simulations were conducted on a single pore network, on multiple networks in series, and by embedding the Berea Sandstone networks in a reservoir simulator using concurrent coupling. The simulations on the single network were used to understand the impact that the alteration of pore structure (caused by particle plugging) has on the dispersion and retention coefficient. The simulations on multiple network models in series (boundary coupled model) were used to verify that it could serve as an adequate validation of the concurrently coupled model and to investigate the particle plugging process at greater length scales. Finally, simulations were conducted on the concurrently coupled model to establish a proof of concept and show that it is a functioning predictive tool.

All of the simulations in this study were conducted using the Berea Sandstone network model discussed previously. The simulations were conducted with constant flow boundary conditions using a Darcy velocity of 0.01 cm/s. A constant fluid viscosity of 0.01 g/cm-s was used for the fluid. All of the injections on the network were conducted in the z-direction to make the injecting face a square cross-sectional area. A summary of the simulation parameters is given in Table 2.

Table 2: Network model simulation parameters held constant for all simulations.

Network Model Simulation Parameters	
3-D Network Model:	Berea Sandstone
Boundary Condition:	Constant Flow Rate
Injection Face:	-z (bottom face)
Darcy Velocity:	0.01 cm/s
Fluid Viscosity:	0.01 g/cm-s

4.1 Single Network Model Results

Particle plugging simulations were carried out in a single Berea Sandstone network model to study the sensitivity of the model to particle size. Simulations were performed to examine the size range of particles that would trap in the network. In addition, simulations were run with multiple particle sizes to examine the effect of injecting particles of different size into the same porous medium. The trapping of particles in the porous medium was dependent on the particle size, the uniformity of the particle size, and the method in which a non-uniform particle size was injected.

The number of particles injected into the porous medium affects the retention and dispersion coefficient, defined in section 3.3.1, if particles are trapped. Particle plugging simulations were run for a uniform particle size to determine the influence that number of particles injected has on the dispersion and retention coefficient. In general, for a uniform particle size, the retention coefficient decreased as the number of particles injected was increased. The following sections discuss the above findings in detail by looking at the results of numerical simulations carried out on a single network model.

4.1.1 Injection of Uniform Particle Sizes

A series of injection simulations were carried out to determine the amount of plugging occurring in the Berea Sandstone network model. In each of these simulations 10,000 spherical particles, uniform in size, were injected in the vertical direction of the core. A total of three pore volumes of fluid were injected during each simulation run. The number of particles passing through the porous medium was recorded for sizes 8 to 19 micron. At first, the same random number seed was used for each of the injection simulations to remove the influence of stochastic particle path selection. The same set of simulations were run a second time using a different random number seed at each run to ensure that averaged results were independent of the stochastic part of the process. The results are shown in the bar chart in Figure 8.

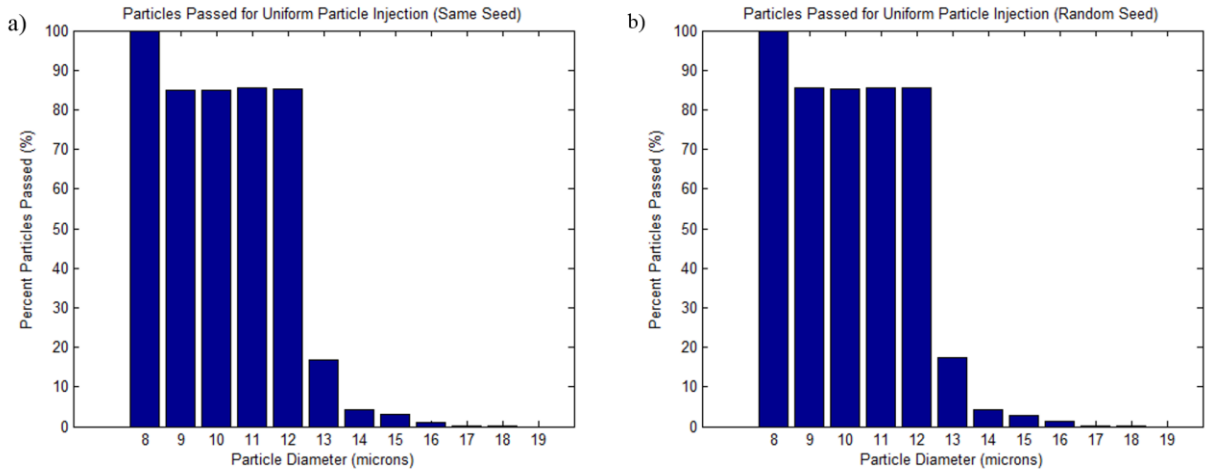

Figure 8: A bar chart of 12 simulations runs injecting 10,000 uniform particles into the Berea Sandstone network model and reporting the number of particles passed per simulation. In (a) the simulations were carried out using the same random number seed in (b) the simulations were carried out using a different random seed.

The two plots show that the random number seed had very little influence on the retention of uniform particles. These charts provided a guide for selecting particle sizes for particle retention simulations on this sample of Berea Sandstone. It is shown that approximately 85% of the 9 through 12 micron particles passed. To understand why the 9 through 12 micron particle size showed approximately the same number of particles retained, the pore throat size distribution was examined for the Berea Sandstone network model.

The pore throat size distribution for the Berea Sandstone network model is shown in Figure 9. Plot (b) shows that the smallest non-zero throat diameter is approximately 8 microns. The next largest throat size is just above 12 microns. This gap in throat size caused the results for the injection of particles in the size range of 9 to 12 microns to yield approximately the same results. Therefore when designing injection simulations of multiple particle sizes, at most one particle species was chosen from the 9 to 12 micron particle diameter.

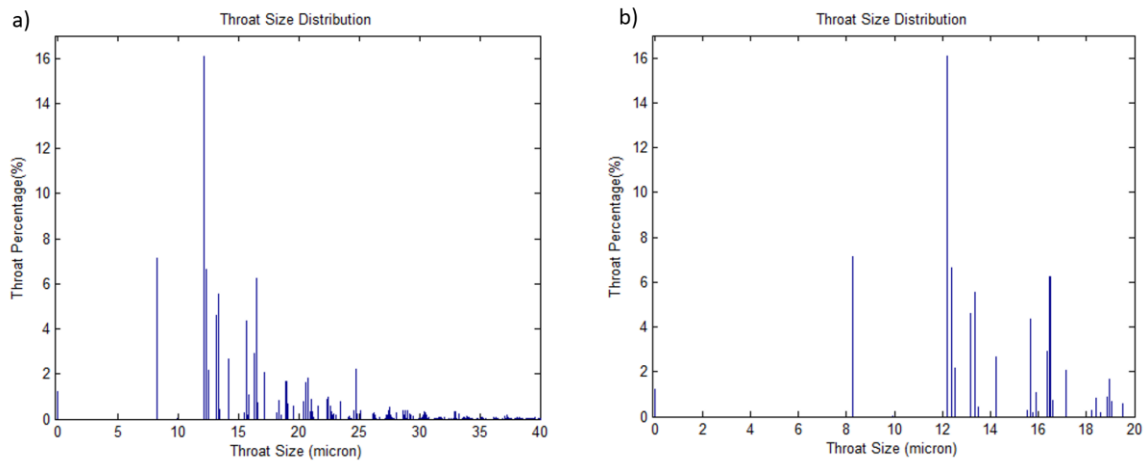

Figure 9: The pore throat size distribution for the Berea Sandstone network model, (a) shows the entire distribution and (b) shows the throats in the range of 0 to 20 microns.

The locations of the trapped particles provide additional observations about the particle plugging process. Three of the uniform particle injection simulations (10, 14, and 18 micron) were selected to visualize the locations of the trapped particles in the Berea Sandstone sample. As stated previously, the particles were injected in the vertical (z) direction starting at z = 0 cm to z = 0.227 cm. The locations of the trapped particles are projected onto the *xz* plane for the three simulations in Figure 10.

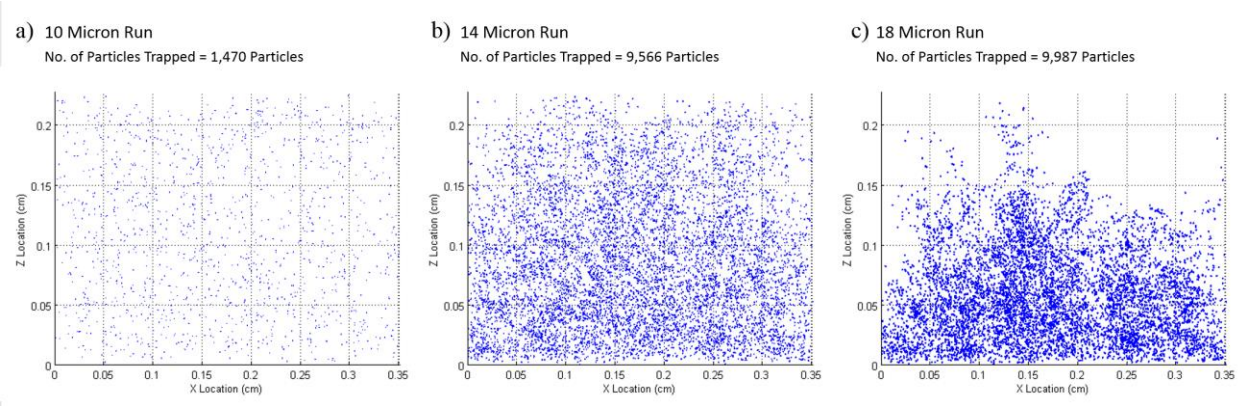

Figure 10: The trapped particle locations for three simulation runs injecting particles in the z direction: (a) 10 micron, (b) 14 micron, (c) 18 micron.

The maps of particle injection show how particle size influenced where the particles are trapped. For the 10 micron diameter, a particle appeared as likely to be trapped near the inlet as near the outlet. This is shown by the even distribution of particles in the cross-section of the Berea Sandstone. For the 14 micron diameter, a particle was more likely to plug near the inlet than the outlet, this is shown by the higher frequency of trapped particles in the first half of the cross section than the second half. For 18 micron diameter, a particle was very likely to plug near the inlet; however over time all of the small throats near the inlet are plugged and the particles began

to travel only through the larger throats. Therefore, particles began to exit the Berea Sandstone at a late point during the injection once the small pore throats had been plugged. Figure 11 shows the trapped particle locations for the 18 micron injection simulation at three points in time during the injection.

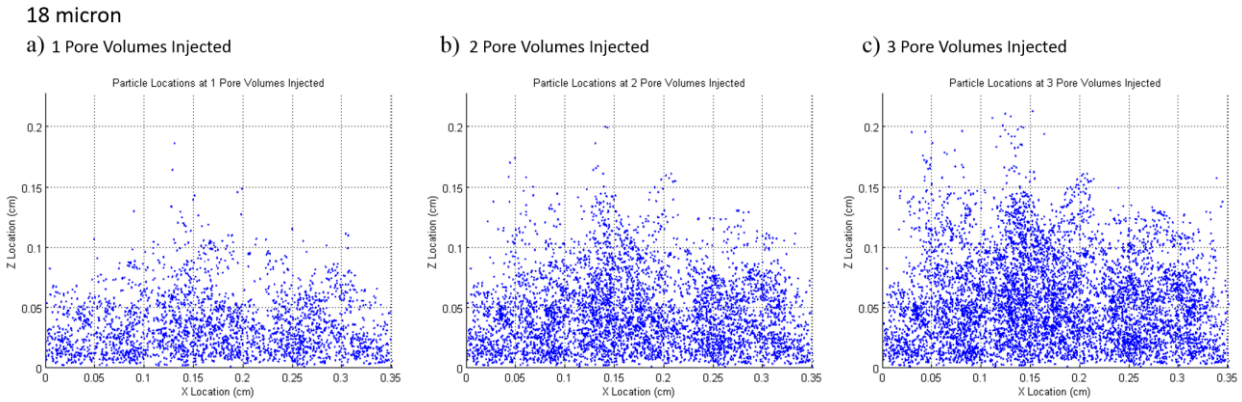

Figure 11: The trapped particle locations for three points in time during an injection of 10,000 (18 micron) particles. The times shown are (a) 1 pore volumes injected, (b) 2 pore volumes injected, (c) 3 pore volumes injected.

The trapped particle location maps show that the 18 micron particles had a greater chance of infiltrating further into the Berea Sandstone as time went on. Eventually, the only remaining open throats were the ones large enough to allow the 18 micron particles to travel through them and the porous medium no longer retained any particles. In general, during particle injection of a single species of uniform size, the porous medium will reach a point where particles are no longer being retained or where the porous medium is completely plugged and will no longer allow fluid flow.

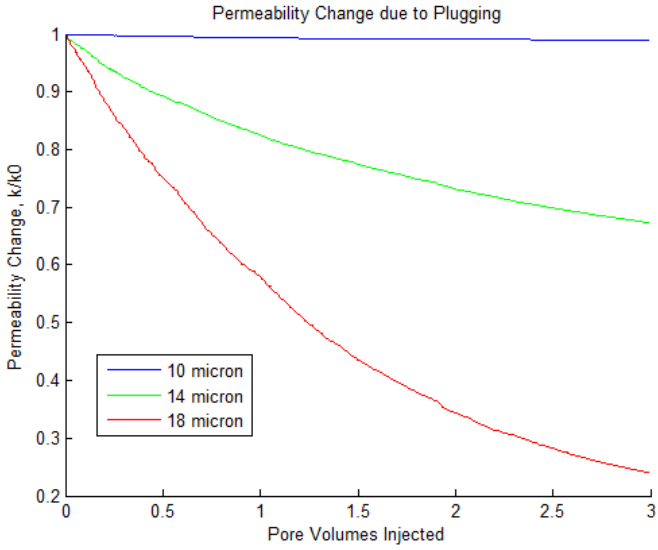

Figure 12: The change in permeability due to particle plugging for three different uniform particle size distributions, 10, 14, and 18 micron.

The plugging of throats causes a reduction in permeability. The more throats that are plugged, the greater the damage to the porous medium, and the steeper the decline in permeability. For a uniform particle species eventually all of the pluggable throats will plug or the permeability will be reduced to zero and fluid can no longer flow. If all the pluggable throats are plugged but particles can still flow through the porous medium, the permeability will cease its decline and remain nearly constant. The permeability plots are shown for the 10, 14, and 18 micron particle injections in Figure 12. The 14 and 18 micron particles permeability curves were still declining at the end of the three-pore-volume injection because all of the pluggable throats had not yet been plugged. The 14 micron particles ceased plugging in new throats early in the injection process and the permeability reduction rate goes to zero.

4.1.2 Number of Particles Injected

The effect of number of particles injected on the dispersion and retention coefficient was investigated by simulating the injection of 10 micron particles through the Berea Sandstone network. Each simulation was conducted with a different number of particles between 1,000 and 1,000,000 particles. The simulations used the same random number seed to ensure that the stochastic nature of the particle path selection did not affect the results. Injecting less than 1,000 particles caused significant scattering in the pore-scale effluent data because the number of expected particles per bin was low. This caused the ratio of actual particles exiting to expected particles exiting to be low resolution. The retention coefficient that was obtained by fitting the CFT model to the scattered data was less accurate due to the scattering. The excessive scattering is shown in Figure 13 for 100 and 500 particle injections.

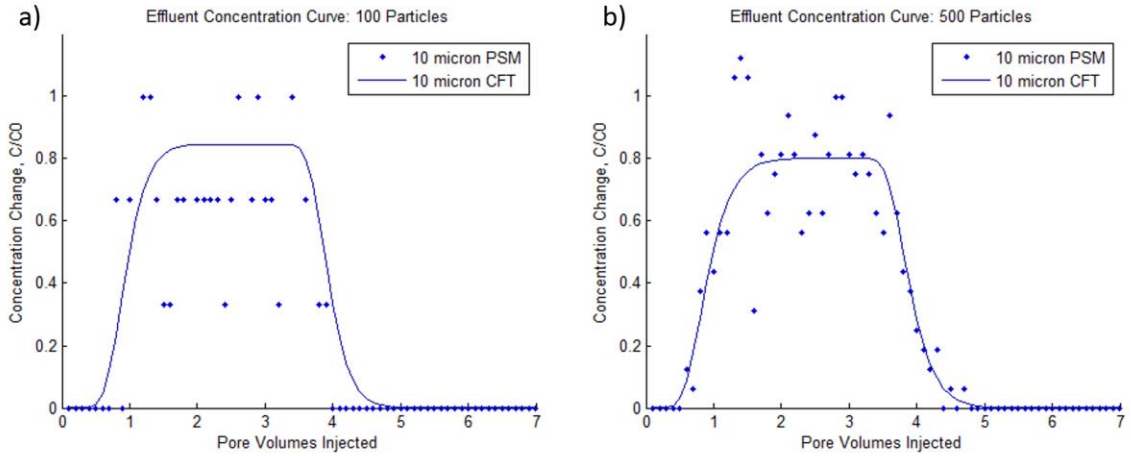

Figure 13: Effluent concentration data scattering due to injection of too few particles. The effluent curves for (a) 100 particles and (b) 500 particles show too much scattering to accurately determine the retention and dispersion coefficient by fitting the CFT model to the data.

The results from eight different 10-micron particle injection simulations were considered. The number of particles injected for the eight simulations were in the range of 1,000 to 1,000,000 particles. The dispersion and retention coefficient was calculated during each simulation and varied depending on the number of particles injected. The two plots in Figure 14 show the

dispersion coefficient (a) and the retention coefficient (b) versus the number of particles injected. At first the dispersion coefficient decreased as the number of particles increased, but for 500,000 or more injected particles, the dispersion coefficient was increasing. This behavior may be counter intuitive if one expected that dispersion decreased as the number of particles was increased because of the reduction in paths that a particle can take due to plugging. The retention coefficient decreased as the number of particles injected was increased. This makes sense for a uniform particle size because eventually all of the pluggable throats for that particle size will have plugged and particles will only flow through the unplugged throats. After enough particles have been injected, the retention coefficient should go to zero for a uniform particle size.

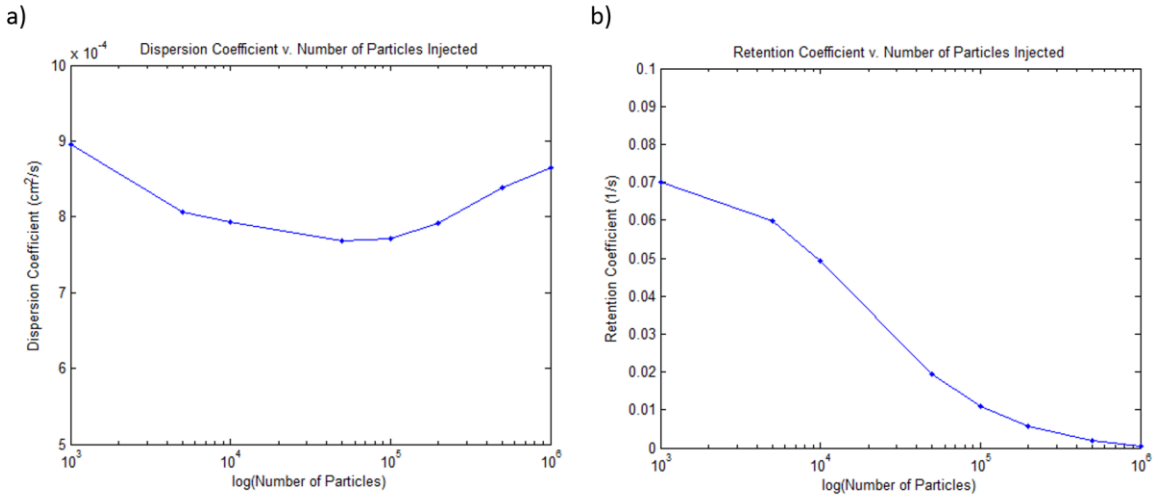

Figure 14: The dispersion (a) and retention (b) coefficient versus the number of particles injected.

While the behavior of the retention coefficient with respect to number of particles injected was as predicted, the change in the dispersion coefficient is not as easily explained. This is possibly due to the fact that the dispersion coefficient changes slightly as the porous medium becomes plugged. In addition, there is a numerical effect in the binning process. As the number of particles is increased, the scattering in the bin data is decreased, this is shown in Figure 13. Therefore, the dispersion coefficient fit to the pore-scale effluent data is also dependent on the scattering caused by the particle binning. To investigate the change in dispersion coefficient caused by permeability damage to the formation (due to particle retention) an additional set of simulations was conducted.

4.1.3 Dispersion Coefficient Response to Formation Damage

A simulation was designed in which a set number of trappable particles (greater than 8 micron) were injected to damage the porous medium. After injecting large particles and damaging the formation, a set number of small particles (0.1 micron) that all pass through the porous medium were injected. For the small particle injection, the dispersion coefficient was recorded and represents the dispersion for the damaged porous medium. By injecting the same set number of

particles at each run, the dispersion coefficient was independent of the scattering caused by the particle binning. These results explain how permeability impairment affects the dispersion coefficient.

In the first set of simulations, 10 micron particles were injected to damage the formation and 0.1 micron particles were injected to determine the dispersion coefficient associated with that damage. In the second set of simulations, 13 micron particles were injected to damage the formation and the dispersion coefficient was determined as discussed previously. In both simulations the damaging particles were injected in increments of 10,000 particles; a total of 50,000 damaging particles were injected. The change in dispersion coefficient (a) and permeability damage (b) with respect to the number of damaging particles injected are shown in Figure 15.

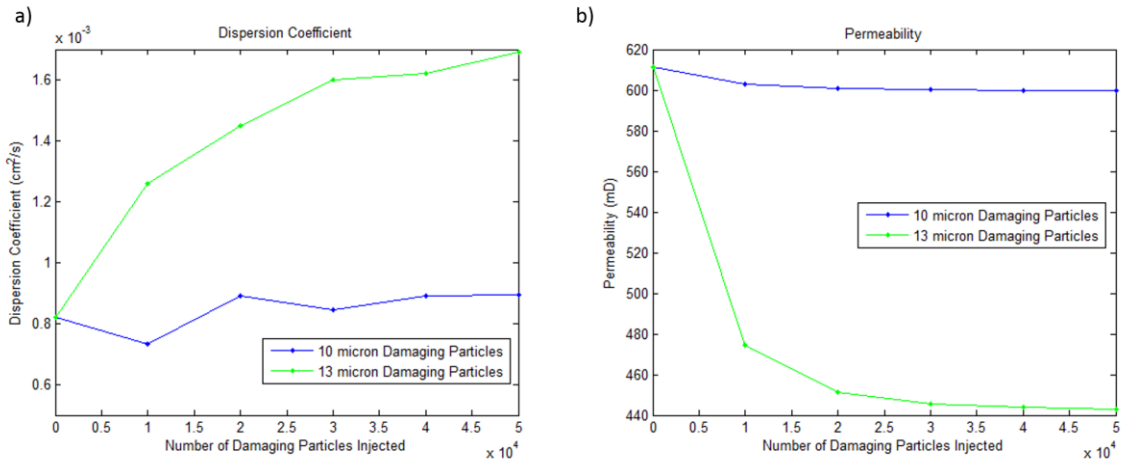

Figure 15: The change in dispersion coefficient (a) and the permeability damage (b) with respect to number of damaging particles injected. 50,000 damaging particles were injected in increments of 10,000 particles.

The results serve as evidence that the dispersion coefficient for the Berea Sandstone sample increases as the formation is damaged. The permeability damage caused by the 13 micron particles was much greater than the damage incurred by the 10 micron particles. The change in dispersion coefficient was related to the magnitude of the permeability impairment. Therefore the greatest increase in dispersion occurred during the period where permeability was rapidly decreasing. To investigate this further, a set of simulations was run to capture the dispersion coefficient change during the time where permeability is rapidly decreasing.

This set of simulations used the same parameters as previously discussed in this section, however the damaged particles were injected in increments of 1,000 particles. In total, 5,000 damaging particles were injected in this set of simulations. By injecting the damaging particles in smaller increments, the simulations captured the change in dispersion coefficient associated with the rapid decline of permeability. The results are shown in Figure 16. The results of the two sets of simulations show the same trend, dispersion coefficient increased as the formation was damaged. The important take away from this study is that for a uniform particle size, the dispersion

coefficient will change the most at early times. At these early times, the permeability is being damaged the most rapidly because the most pore throats are still available to being plugged. Once the formation is significantly plugged, the permeability will no longer be damaged and particles will flow mostly through large unplugged throats and the dispersion coefficient will remain relatively constant. In these two sets of simulations the dispersion coefficient increase was related to the rate that the formation permeability was damaged.

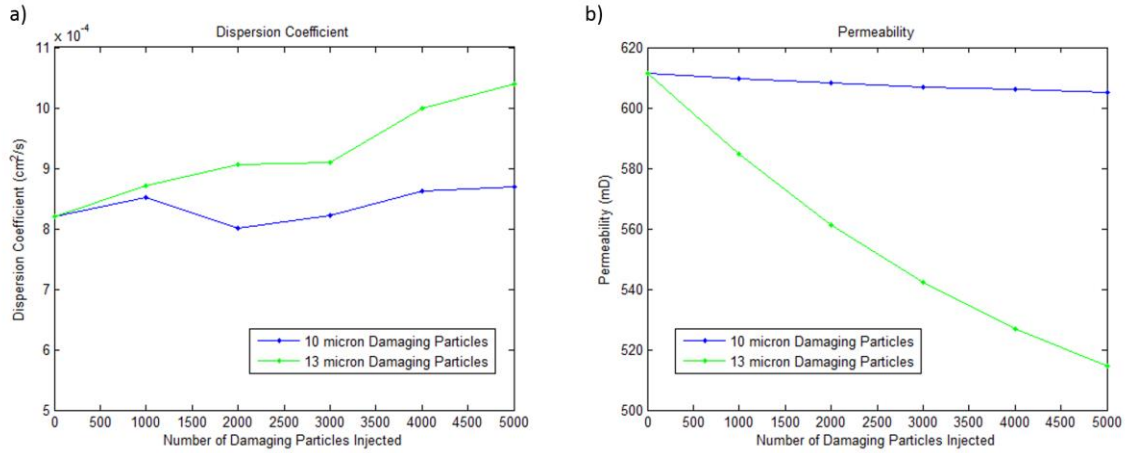

Figure 16: The change in dispersion coefficient (a) and the permeability damage (b) with respect to number of damaging particles injected. 5,000 damaging particles were injected in increments of 1,000 particles.

4.1.4 Multiple Particle Species Injection

Injecting multiple particle species of different diameter has an effect on the retention of each particle species. Furthermore, how one injects these particles influences the retention of each species. A different number of particles will be retained for an injection situation where two particle species are injected simultaneously (in parallel) versus injecting the two species one after another (in series). The difference in retention caused by injecting multiple particle sizes and the order in which one injects them cannot be detected by an empirical relationship or continuum-scale model. The pore-scale particle plugging simulator was used to examine the effects of multiple species particle injection on retention.

The particle plugging simulator was run for three cases, (1) injection of 10 micron particles first and 13 micron particles second, (2) injection of 13 micron particles first and 10 micron particles second, and (3) the simultaneous injection of 10 and 13 micron particles. The particle sizes were chosen based on their retention when injected in separate simulations. 85% of the 10 micron particles pass, while 18% of the 13 micron particles pass. These two sizes were selected for this example because most of the 10 micron particles pass and most of the 13 micron particles are retained. The effluent curves for the three cases are shown in Figure 17 along with a summary of the retention data. The data points represent the pore-scale model results and the lines represent the fitted CFT model.

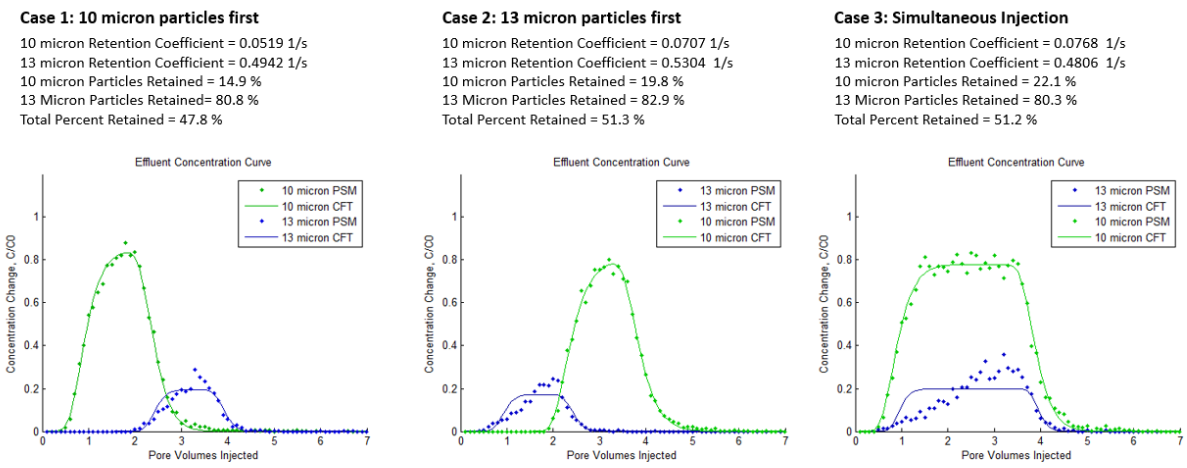

Figure 17: The effluent concentration curves for three two particle species injections cases, (1) 10 micron particles first and 13 micron particles second, (2) 13 micron particles first and 10 micron second, (3) simultaneous injection of 10 and 13 micron particles.

The total percent of particles retained is different for each of the three plots. The lowest percent of particles were retained in case 1 and the greatest percent of particles were retained in case 2. In addition, the retention coefficient for each species was different in each injection case. Only the pore-scale model can capture the effect of the particle species injection scheme. The pore-scale plugging simulator was necessary for the prediction of each case's unique retention coefficient. For simplicity, this example only showed two sets of particle sizes, but the model can be run for any number of particle species (diameters). This simple set of two particle species injection simulations shows the utility and necessity of the pore-scale simulator when determining the retention coefficients used in a reservoir scale gridblock.

4.2 Multiple Network Models Results

Particle injection simulations were conducted on multiple network models connected in series to study the effect that the length of the porous medium had on particle retention and dispersion. It was also used to test whether the dispersion and retention coefficients obtained from a single network can be used to predict the particle breakthrough times and concentration change across greater lengths. In addition, running simulations on multiple networks and comparing to coupled simulations with the same number of continuum gridblocks served as a validation of the coupled simulator. A variety of simulations of particle injections through multiple gridblocks in series are discussed in the following sections.

4.2.1 Effect of Increasing Sample Length

By injecting particles into multiple network models in series, we are able to investigate how increased sample length affects the particle dispersion and retention. It is expected that by increasing the length of the porous medium, more particles will be retained and particle

breakthrough time will be delayed. The boundary coupled model is able to predict these effects and several simulations discussed in this section explain them.

A set of simulations was run to verify the effects of increasing the sample length by injecting through multiple coupled networks. In these simulations, non-plugging particles (0.1 micron) were injected into 1, 5, and 20 networks in series with the sample lengths of 0.23 cm, 1.15 cm, and 4.60 cm respectively. Figure 16 shows that as the number of networks (length) is increased, it takes longer for the first particles to exit the formation as expected.

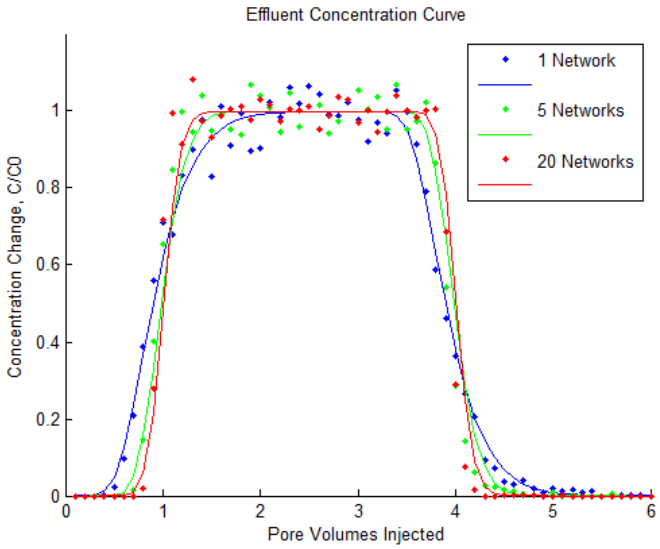

Figure 18: The effluent concentration curves from 3 simulations on 1, 5, and 20 networks in series.

One should keep in mind that the pore volume of the sample increases as the number of networks is increased. Time is presented as pore volumes injected; therefore it scales in proportion to the size of the network and the delay shown on the plot is caused by the diminishing effect of dispersion over greater lengths. For non-plugging particles, as one increases the length of the same sample, eventually the effluent curve will take on the same shape for any length of material for the same number of pore volumes injected.

To test the ability of the boundary coupled model to simulate the increased retention caused by the increase in the porous medium length, 10 micron particles were injected into five networks in series. To visualize the increase in particle retention, the effluent concentration curve of each network in series was plotted in Figure 19.

The plot shows that the model captures the increase in retention. However it is important to keep in mind that the retention coefficient for all 5 networks is expected to be the same. Particle retention increases as sample length increases, but the retention coefficient of that sample remains the same (because the pore structure in each of the five networks is identical). If particles were injected into several different models in series, the particles' retention coefficient would vary from network to network, but the fraction of particles retained would still increase as

particles flow through a greater number of networks, unless they were non-plugging particles that have a retention coefficient of zero.

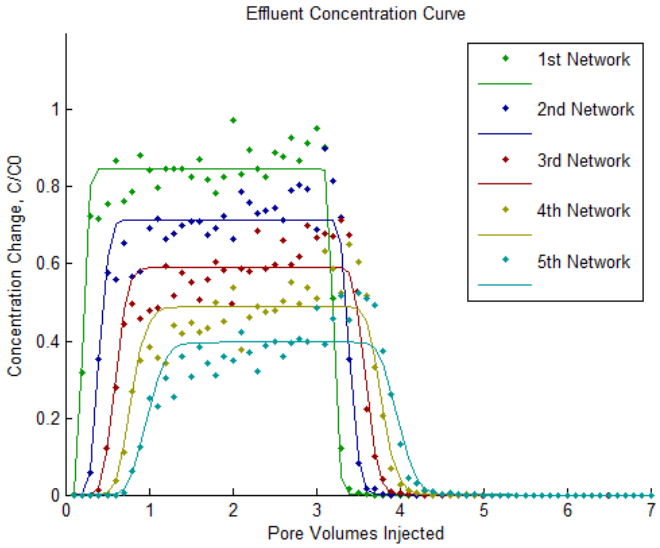

Figure 19: The effluent concentration curve produced by each of the 5 networks connected in series. The curve shows the increasing retention of particles at each increase in length.

4.2.2 Dispersion Coefficient from Multiple Networks

The dispersion coefficient of a given porous medium should remain constant if that porous medium is not being damaged by plugging particles. The total amount of longitudinal dispersion will scale with length, but the dispersion coefficient for a particle in an unchanging porous medium should remain constant. The dispersion coefficient obtained from one network model with non-plugging particles should be the same as the dispersion coefficient obtained from multiple network models coupled in series.

Several simulations were run to test the validity of the method used to link multiple network models in series. The simulations were run by injecting small non plugging particles (0.1 micron) into 1, 2, 5, 10, 15, 20, 25, and 30 network models in series. The number of networks in series represents the following lengths respectively 0.23 cm, 0.46 cm, 1.15 cm, 2.30 cm, 3.45 cm, 4.60 cm, 5.75 cm, and 6.90 cm. The results showed that the dispersion coefficient varied between a minimum of 0.0087 cm^2/s and 0.013 cm^2/s with an average of 0.011 cm^2/s. All of the results are shown in Figure 20. We believe the variation in dispersion coefficient is a result of the simplistic boundary coupling method used to link the network models. In this method, the particles passing from one network are randomly injected into the next network in series. To be more realistic, a more rigorous boundary coupling method should be used to determine where the exiting particles are reinjected at the inlet face of the next network in series.

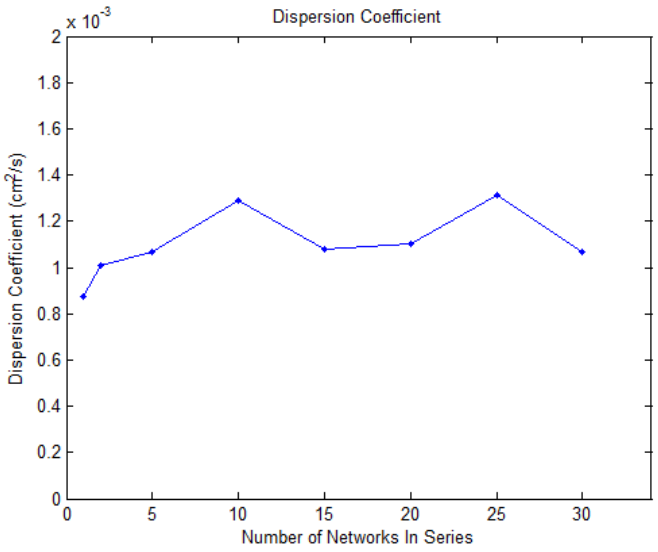

Figure 20: The dispersion coefficient resulting from the injection of the same number of particles into different numbers of network models in series to represent increasing sample length.

The amount of variation shown in the dispersion coefficient for the simple boundary coupling method is acceptable. It will not have a tremendous impact on the particle breakthrough time for the boundary coupled model. This is shown by Figure 21 in which effluent curves were generated using the minimum, average, and maximum calculated dispersion coefficient from the multiple networks-in-series calculations. These effluent curves were generated for the same size porous medium; therefore if the dispersion coefficient was constant the three curves would be identical.

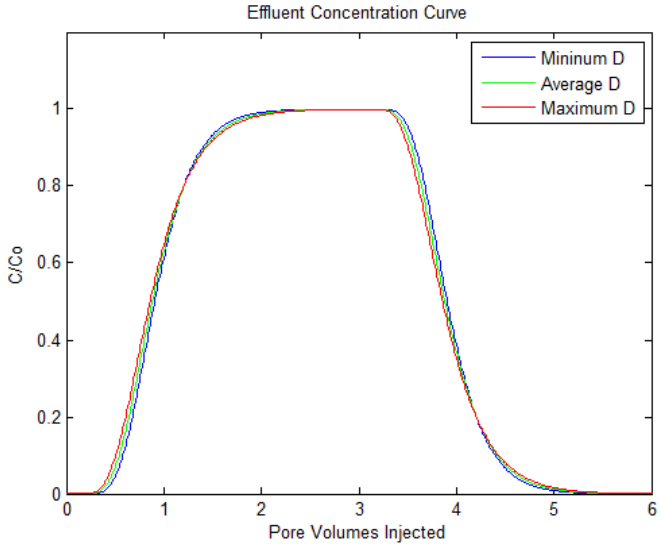

Figure 21: Effluent curves generated from the minimum, average, and maximum dispersion coefficients obtained from a series of simulations injecting the same number of particles into a different number of network models in series. Each curve represents the same length.

Furthermore the variation in the dispersion coefficient is acceptable because the breakthrough time of particles is more strongly influenced by the length of the sample. This is shown in Figure 22 in which effluent curves represent the dispersion coefficients obtained for 1, 5, and 20 network models and their respective lengths of 0.23 cm, 1.15 cm, and 4.60 cm. The effluent curves are shown for the same number of pore volumes injected of the 3 different model sizes. The resulting effluent curves show that particle breakthrough nondimensional time (pore volumes injected) is increased as length of the porous medium is increased due to the greater amount of dispersion.

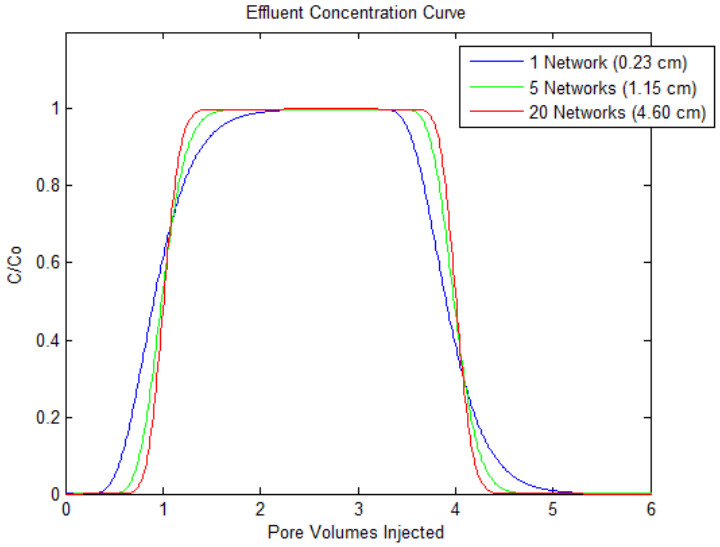

Figure 22: The effluent curves generated from dispersion coefficients obtained from 1, 5, and 20 networks and their respective lengths 0.23 cm, 1.15 cm, and 4.6 cm.

The purpose of this section is to justify the validity of the boundary coupling method. For testing the concurrently coupled model and studying the use of continuum-scale coefficients at greater lengths, the variance in the dispersion coefficient is acceptable. For a more detailed study of the longitudinal dispersion coefficient, it is recommended that the particle transport at boundaries is rigorously determined to decrease variation in the dispersion coefficient across multiple networks.

4.2.3 Validation of the CFT Model at Greater Lengths

One of the major concerns for coupling the pore-scale simulator with the field scale is the use of a continuum-scale parameter obtained at a very small scale to solve a much larger scale problem. In this study, it is important that we confirm that the retention coefficient obtained from a single network model can be used to accurately predict particle retention across greater spatial scales in the reservoir simulator. To test this concept, particles were injected in multiple network models in series (as a means to increase the length of the sample). The CFT model was run using a retention and dispersion coefficient obtained from a single network model (but applied to various physical sizes) and the results were compared with the multiple network results.

A uniform particle size of 10 microns was injected into 10 network models in series. The retention and dispersion coefficient were obtained from a single network model injecting the same number of 10 micron particles. The CFT model was run using the retention and dispersion coefficient from the single network model but using the length represented by the 10 network models in series, 2.27 cm. The effluent curves produced by the 10 network models in series and the CFT model were compared. As concluded previously, the retention coefficient is dependent on the number of particles injected and therefore we ran separate sets of the simulations described above injecting 10,000, 100,000, and 1,000,000 particles. The effluent curves from the three sets of simulations are shown in Figure 23.

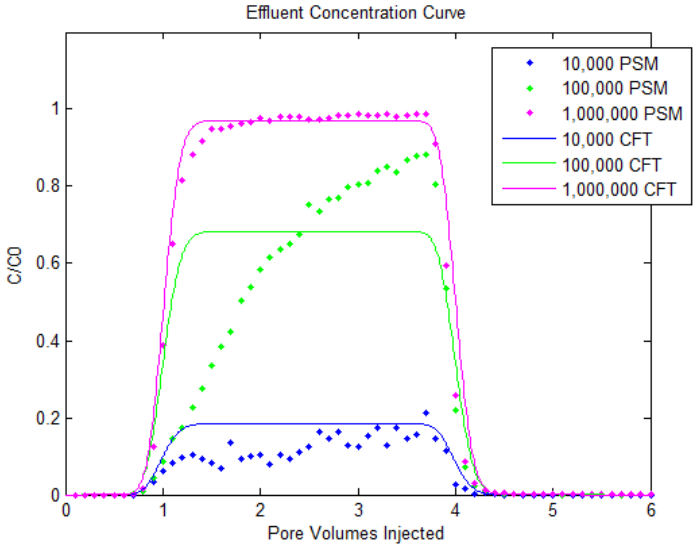

Figure 23: The effluent curves produced by three sets of simulations injecting different number of particles into ten network models in series and comparing the results to the CFT model using a dispersion and retention coefficient obtained from a single network model.

The CFT model is clearly a simplification of the particle plugging occurring over the 2.27 cm. The overall shape of the CFT effluent curve does not line up with the shape of the pore-scale model results. Despite the difference in shape, the two models predict approximately the same amount of particles plugging. This suggests that using a retention and dispersion coefficient obtained from a single network can be used in the continuum-scale model to represent particle retention across greater lengths. This is an important confirmation for running coupled simulations where a network model is embedded in a continuum-scale gridblock that is much greater in length.

An additional observation is the effect of the number of particles injected for a uniform particle size. As discussed previously the retention coefficient of a uniform particle size decreases with respect to the number of particles injected. That is why the results for the ten network pore-scale model and CFT model show an increasing maximum C/C_0 with respect to number of particles injected. Referring back to Figure 14, it is evident that there is a large change in the retention coefficient when the number of particles injected is between 5,000 and 100,000 particles. It is important to consider this transient behavior of the retention coefficient when running the

coupled simulations. For instance if the time-steps are too large in the coupled simulation (and if this is used to dictate the number of particles injected at the pore-scale), the number of particles injected might be so large that the retention coefficient predicted by the network model will be close to zero. In this case, the dynamic nature of the retention coefficient would be missed and the reservoir simulator will fail to include the transient behavior of the particle plugging process.

4.3 Concurrently Coupled Model Results

The primary goal of this work is to prove that the concurrent communication between the pore-scale particle plugging simulator and the reservoir simulator is working. For this purpose, the concurrently coupled model is used in a simple domain where the continuum-scale gridlocks are the same dimensions as the actual network model. Five network models are coupled to five continuum-scale gridblocks. At the continuum-scale, the simulator is operated in time steps equivalent to injecting one network pore volume of fluid. The continuum-scale model dictates the particle size, suspension concentration, fluid viscosity, and fluid velocity of the injected fluid in the coupled pore-scale models.

4.3.1 Pressure Response to Permeability Change

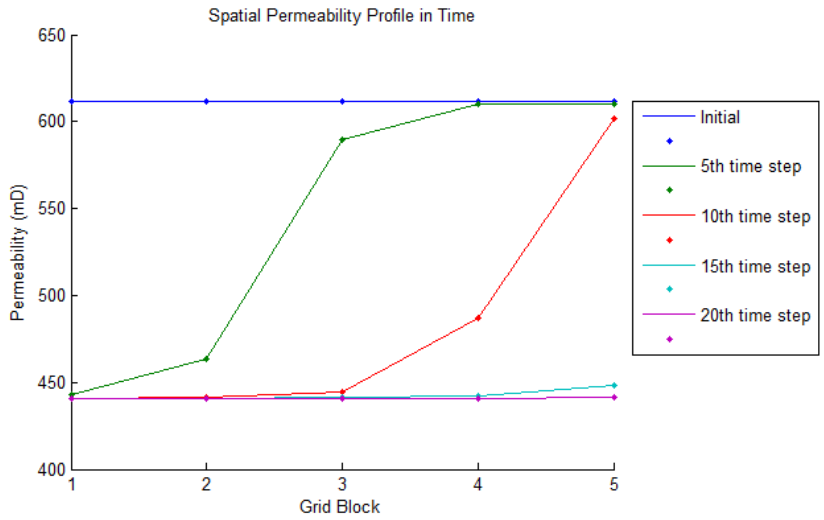

Figure 24: The spatial permeability profile in time for a 13 micron particle injection at time steps equivalent to injecting 1 pore volume of fluid with 10,000 particles suspended.

Available results show the change in permeability and change in pressure in the model when subjected to a constant rate injection of 13 micron particles. At each time step one network or gridblock pore volume of fluid was injected with a total of 10,000 particles suspended. One network pore volume was equivalent to 0.2 total system pore volumes. The permeability declined first in the gridblock closest to the injection point but eventually reached a point in all the gridlocks where it is no longer declining as seen previously. For a constant rate injection of

particles, the pressure in a grid block increased as the formation was damaged by particles and the permeability was impaired.

The spatial change in permeability for several time steps is shown in Figure 24. Initially the permeability was equal for the 5 grid blocks. After the 5th time step, the first gridblock reached its final permeability and particles were no longer being trapped. At this same point in time, particles had significantly damaged the second gridblock and traveled into the third gridblock. At the 20th time step almost all of the gridblocks were damaged to the full extent that that could occur for uniform 13 micron particles. In this case where a uniform particle size was injected, the porous medium reached its maximum amount of damage very quickly. In addition, these results confirm that the coupling works and the network model passes the time dependent permeability to the continuum-scale model. It is encouraging that the permeability trend in the coupled model is the same as what a single network model shows for a uniform particle size: permeability declines to a certain point and then remains constant.

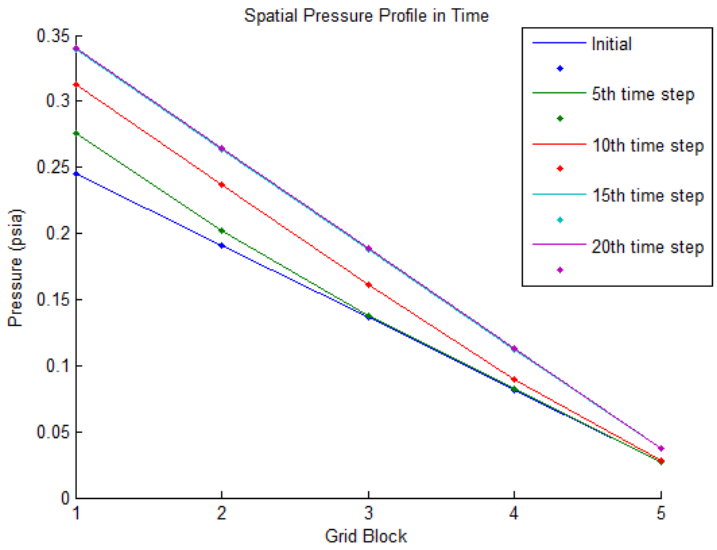

Figure 25: The spatial pressure profile in time for a 13 micron particle injection at time steps equivalent to injecting one pore volume of fluid with 10,000 particles suspended.

The spatial change in pressure for several time steps is shown in Figure 25. The pressure profile shows a constant decline in pressure for the initial time because the permeability was the same in all the gridblocks. This is the same pressure decline that could be predicted by Darcy's law since the permeability, flow rate, viscosity, cross sectional area, and elevation remain constant. By the 5th time step, the pressure increased in the first and second gridblocks in response to the permeability reduction. Eventually, the permeability in all the gridblocks was reduced and the pressure in all of the gridblocks was increased, as did the overall pressure drop across the model. Once again this behavior can be explained by considering Darcy's law where the pressure drop is inversely proportional to permeability. As the permeability was reduced in the model, the pressure drop increased. The agreement between the model results and Darcy's law is further evidence that the concurrent coupling is working properly.

4.3.2 Validation of the Concurrently Coupled Model

The concurrently coupled model was validated using the boundary coupled model. Each model was run under the same conditions. Both models simulated the injection of four total system pore volumes of a suspension with a uniform particle size distribution. The models both simulated flow through a sample five times the length of one network model. Therefore the continuum-scale gridlocks in the concurrently coupled model were the same size as the network model. The two models represented two different approaches to modeling the same system and therefore their results should agree.

To compare the two models, an effluent curve was produced from each model. For the first comparison case, 200,000 ten-micron particles were injected into both models in four total system pore volumes of fluid. The concurrent model was operated at time steps equal to one network pore volume or 0.2 system pore volumes. The particle binning for the coupled model was carried out using 0.1 system pore volume bins, therefore the boundary coupled model produced double the data points for higher resolution. The results of the two models are shown in Figure 26.

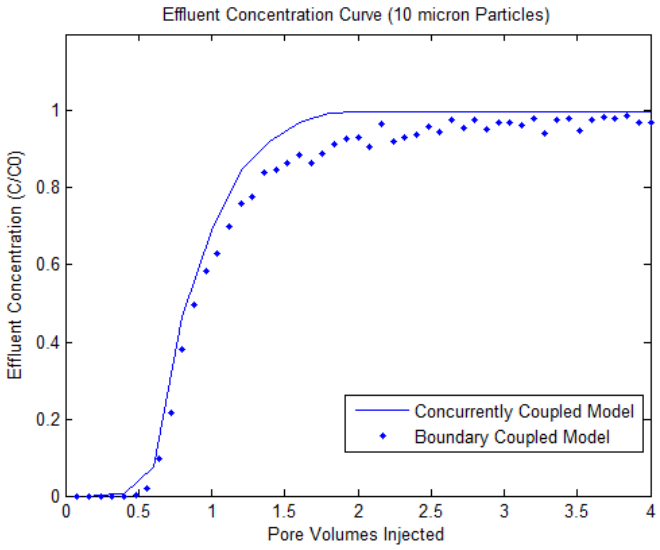

Figure 26: The effluent concentration curves generated from the concurrently coupled model (5 grid blocks) and the boundary coupled model (5 networks in series).

The results are in agreement and suggest that the preliminary implementation of the coupled model is working properly. The slight difference in the two curves is possibly caused by the particle binning. If only a few particles are being injected into a gridblock due to retention in the other blocks, the particle binning will cause significant scattering as discussed previously in section 4.1.2. The fitting of the CFT model to this scattered data will yield an inaccurate determination of the retention coefficient. In addition, if the concurrently coupled model were run at smaller time steps it should show better agreement with the boundary coupled effluent data. Overall the match serves as a proof of concept and shows that the concurrent communication between the two simulators is working properly.

CHAPTER 5. CONCLUSION

This work presents the development and use of a multiscale particle transport simulator. The concurrently coupled model captures the dynamic behavior of the dispersion and retention coefficient observed at the pore-scale. Previous works (Rhodes and Blunt, 2006) have noted the significant impact that pore-scale structure has on the particle transport process at the field scale. At the pore-scale previous works (Meloy et al., 1991; Sharma and Yortsos, 1987) have identified that particle dispersion and retention is dependent on time and space as well as the size of the particles. This study aimed to investigate the particle plugging process at the pore-scale to qualitatively and quantitatively validate the concurrently coupled model. The following conclusions were determined from pore-scale simulations:

1. The retention coefficient for a uniform particle size will decrease as the number of particles injected increases due to the fact that all of the pluggable throats become plugged and eventually particles are no longer retained. The permeability will show corresponding behavior: at first it will damage at a high rate, but eventually the permeability will reach a minimum and show no further damage. Finally, for a uniform particle size the magnitude of damage associated with particle plugging is dependent on the particle size.
2. The dispersion coefficient for a uniform particle size will increase as the formation is damaged. The increase in the dispersion coefficient is related to the rate of permeability damage. As permeability damage rate declines, the dispersion coefficient becomes constant.
3. Injecting multiple particle species yields a different dispersion and retention coefficient for each species. Additionally, the continuum-scale coefficients for each species depend on how the particle species were injected. Injecting multiple species simultaneously versus in order of size will yield different dispersion and retention coefficients for each species.

These pore-scale observations demonstrate the importance of including the pore structure in the determination of continuum-scale parameters. Not only will the parameters vary based on the three conclusions above, but they will be different for every porous medium. The true power of the particle plugging simulator is its ability to predict the particle transport continuum-scale parameters for any porous medium, any particle species, and most importantly as the porous medium changes due to particle retention.

The boundary coupled model was used to study the effect of increasing length on particle retention and dispersion. As expected, for a longer sample of the same material, more particles will be retained, but the retention coefficient remains the same at a given time. If particles are not retained, the dispersion coefficient is expected to remain constant despite the increase in sample length. However, due to the random injection of particles at the boundary and the scattering caused by the binning method, the dispersion coefficient values oscillated around a mean value with an acceptable variance. The boundary coupled model determined that continuum-scale parameters obtained from a single network can be used to model retention at greater lengths.

The concurrently coupled model was tested. The model showed that it was able to affectively capture the changes in permeability caused by particle plugging. The loss in permeability caused

increased pressure drop across the system as dictated by Darcy's law. The effluent curves from the boundary coupled model and concurrently coupled model were compared and showed an acceptable level of agreement. This offers assurance that the concurrent coupling method developed in this work is viable.

This study and previous work have observed that particle transport is a pore-scale process and therefore in certain cases field scale studies should include the dynamic behavior of particles at the pore-scale. The true value in this work is not the quantitative data presented, but the two tools that can be used to study particle transport at multiple scales. Both the boundary coupled model and concurrently coupled model offer the ability to incorporate pore-scale physics at greater lengths. The models are robust and allow the use of any number of particle species unlike experiments or empirical equations. With further development the concurrently coupled model will have the ability to predict field-scale particle transport while including the time-dependent dispersion coefficient, retention coefficient, permeability, and porosity obtained from the pore-scale model. This work also serves as a guideline for coupling more complex pore-scale network or finite element models with field scale simulators.

REFERENCES

Balhoff, M. T., Thomas, S. G., and Wheeler, M. F., 2008, Mortar coupling and upscaling of pore-scale models: Computational Geosciences, v. 12, no. 1, p. 15-27.

Balhoff, M. T., Thompson, K. E., and Hjortsø, M., 2007, Coupling pore-scale networks to continuum-scale models of porous media: Computers & Geosciences, v. 33, no. 3, p. 393-410.

Battiato, I., Tartakovsky, D. M., Tartakovsky, A. M., and Scheibe, T. D., 2011, Hybrid models of reactive transport in porous and fractured media: Advances in Water Resources, v. 34, no. 9, p. 1140-1150.

Blunt, M., and King, P., 1991, Relative permeabilities from two- and three-dimensional pore-scale network modelling: Transport in Porous Media, v. 6, no. 4, p. 407-433.

Blunt, M. J., Jackson, M. D., Piri, M., and Valvatne, P. H., 2002, Detailed physics, predictive capabilities and macroscopic consequences for pore-network models of multiphase flow: Advances in Water Resources, v. 25, no. 8–12, p. 1069-1089.

Bryant, S. L., Mellor, D. W., and Cade, C. A., 1993, Physically Representative Network Models of Transport in Porous-Media: Aiche Journal, v. 39, no. 3, p. 387-396.

Carman, P. C., 1937, Fluid Flow Through Granular Beds: Transactions, Institution of Chemical Engineers, v. 15, p. 150-166.

Celia, M. A., Rajaram, H., and Ferrand, L. A., 1993, A multi-scale computational model for multiphase flow in porous media: Advances in Water Resources, v. 16, no. 1, p. 81-92.

Chatzis, I., and Dullien, F. A. L., 1977, Modelling Pore Structure By 2-D And 3-D Networks With ApplicationTo Sandstones: Journal of Canadian Petroleum Technology v. 16, no. 1, p. 97-108.

Chen, C., Packman, A. I., Zhang, D., and Gaillard, J.-F., 2010, A multi-scale investigation of interfacial transport, pore fluid flow, and fine particle deposition in a sediment bed: Water Resources Research, v. 46, no. 11, p. 1-12.

Chu, J., Engquist, B., Prodanović, M., and Tsai, R., 2012, A Multiscale Method Coupling Network and Continuum Models in Porous Media I: Steady-State Single Phase Flow: Multiscale Modeling & Simulation, v. 10, no. 2, p. 515-549.

Chu, J., Engquist, B., Prodanović, M., and Tsai, R., 2013, A Multiscale Method Coupling Network and Continuum Models in Porous Media II—Single- and Two-Phase Flows, *in* Melnik, R., and Kotsireas, I. S., eds., Advances in Applied Mathematics, Modeling, and Computational Science, Volume 66, Springer US, p. 161-185.

Donaldson, E. C., Baker, B. A., and Carroll, H. B., 1977, Particle Transport In Sandstones, Society of Petroleum Engineers.

Dullien, F. A. L., 1975, New network permeability model of porous media: AIChE Journal, v. 21, no. 2, p. 299-307.

Fatt, I., 1956, The Network Model of Porous Media, Society of Petroleum Engineers.

Golzar, M., Saghravani, S. F., and Moghaddam, M. A., 2014, Experimental Study and Numerical Solution of Poly Acrylic Acid Supported Magnetite Nanoparticles Transport in a One-Dimensional Porous Media: Advances in Materials Science and Engineering, p. 4-6.

Hazen, A., 1892, Annual Report Massachusetts State Board of Health: Published Document 34, p. 539.

Heiba, A. A., Jerauld, G. R., Davis, H. T., and Scriven, L. E., 1986, Mechanism-Based Simulation of Oil Recovery Processes, Society of Petroleum Engineers.

Hoefner, M. L., and Fogler, H. S., 1988, Pore evolution and channel formation during flow and reaction in porous media: AIChE Journal, v. 34, no. 1, p. 45-54.

Imdakm, A. O., and Sahimi, M., 1987, Transport of large particles in flow through porous media: Physical Review A, v. 36, no. 11, p. 5304-5309.

Imdakm, A. O., and Sahimi, M., 1991, Computer simulation of particle transport processes in flow through porous media: Chemical Engineering Science, v. 46, no. 8, p. 1977-1993.

Jackson, M. D., Valvatne, P. H., and Blunt, M. J., 2003, Prediction of wettability variation and its impact on flow using pore- to reservoir-scale simulations: Journal of Petroleum Science and Engineering, v. 39, no. 3–4, p. 231-246.

Kozeny, J., 1927, Ueber kapillare Leitung des Wassers im Boden: Sitzungsber Akad. Wiss., Wien, v. 136, no. 2a, p. 271-306.

Lichtner, P. C., and Kang, Q., 2007, Upscaling pore-scale reactive transport equations using a multiscale continuum formulation: Water Resources Research, v. 43, no. 12.

Mathews, J. H., and Fink, K. D., 2004, Numerical Methods Using MATLAB, Pearson.

Mehmani, Y., and Balhoff, M. T., 2014, Bridging from Pore to Continuum: A Hybrid Mortar Domain Decomposition Framework for Subsurface Flow and Transport: Multiscale Modeling & Simulation, v. 12, no. 2, p. 667-693.

Mehmani, Y., Sun, T., Balhoff, M. T., Eichhubl, P., and Bryant, S., 2012, Multiblock Pore-Scale Modeling and Upscaling of Reactive Transport: Application to Carbon Sequestration: Transport in Porous Media, v. 95, no. 2, p. 305-326.

Meloy, T. P., Rulke, A. W., Williams, M., and Aminian, K., 1991, Simulation of Particle Movement in Porous Rock, Society of Petroleum Engineers.

Ochi, J., and Vernoux, J.-F., 1999, A Two-Dimensional Network Model to Simulate Permeability Decrease Under Hydrodynamic Effect of Particle Release and Capture: Transport in Porous Media, v. 37, no. 3, p. 303-325.

Rege, S. D., and Fogler, H. S., 1987, Network Model for Straining Dominated Particle Entrapment in Porous-Media: Chemical Engineering Science, v. 42, no. 7, p. 1553-1564.

Rhodes, M. E., Bijeljic, B., and Blunt, M. J., 2008, Pore-to-field simulation of single-phase transport using continuous time random walks: Advances in Water Resources, v. 31, no. 12, p. 1527-1539.

Rhodes, M. E., and Blunt, M. J., 2006, An exact particle tracking algorithm for advective-dispersive transport in networks with complete mixing at nodes: Water Resources Research, v. 42, no. 4.

Sahimi, M., and Imdakm, A. O., 1991, Hydrodynamics of particulate motion in porous media: Physical Review Letters, v. 66, no. 9, p. 1169-1172.

Salter, S. J., and Mohanty, K. K., 1982, Multiphase Flow in Porous Media: I. Macroscopic Observations and Modeling, Society of Petroleum Engineers.

Schlicter, C. S., 1899, 19th Annual Report Part II: U.S. Geological Survey, p. 301.

Sharma, M. M., and Yortsos, Y. C., 1987, A network model for deep bed filtration processes: AIChE Journal, v. 33, no. 10, p. 1644-1653.

Sheng, Q., and Thompson, K., 2013, Dynamic coupling of pore-scale and reservoir-scale models for multiphase flow: Water Resources Research, v. 49, no. 9, p. 5973-5988.

Siqueira, A. G., Bonet, E. J., and Shecaira, F. S., 2003, A 3D Network Model of Rock Permeability Impairment Due to Suspended Particles in Injection Water, Society of Petroleum Engineers.

Sun, W. C., Andrade, J. E., and Rudnicki, J. W., 2011, Multiscale method for characterization of porous microstructures and their impact on macroscopic effective permeability: International Journal for Numerical Methods in Engineering, v. 88, no. 12, p. 1260-1279.

Thompson, K. E., and Fogler, H. S., 1997, Modeling flow in disordered packed beds from pore-scale fluid mechanics: Aiche Journal, v. 43, no. 6, p. 1377-1389.

Todd, A. C., Somerville, J. E., and Scott, G., 1984, The Application of Depth of Formation Damage Measurements in Predicting Water Injectivity Decline, Society of Petroleum Engineers.

Tsakiroglou, C., 2012, A Multi-Scale Approach to Model Two-Phase Flow in Heterogeneous Porous Media: Transport in Porous Media, v. 94, no. 2, p. 525-536.

Van den Akker, H. E. A., 2010, Toward A Truly Multiscale Computational Strategy For Simulating Turbulent Two-Phase Flow Processes: Industrial & Engineering Chemistry Research, v. 49, no. 21, p. 10780-10797.

White, J., Borja, R., and Fredrich, J., 2006, Calculating the effective permeability of sandstone with multiscale lattice Boltzmann/finite element simulations: Acta Geotechnica, v. 1, no. 4, p. 195-209.

APPENDIX. SIMULATOR FLOWCHART

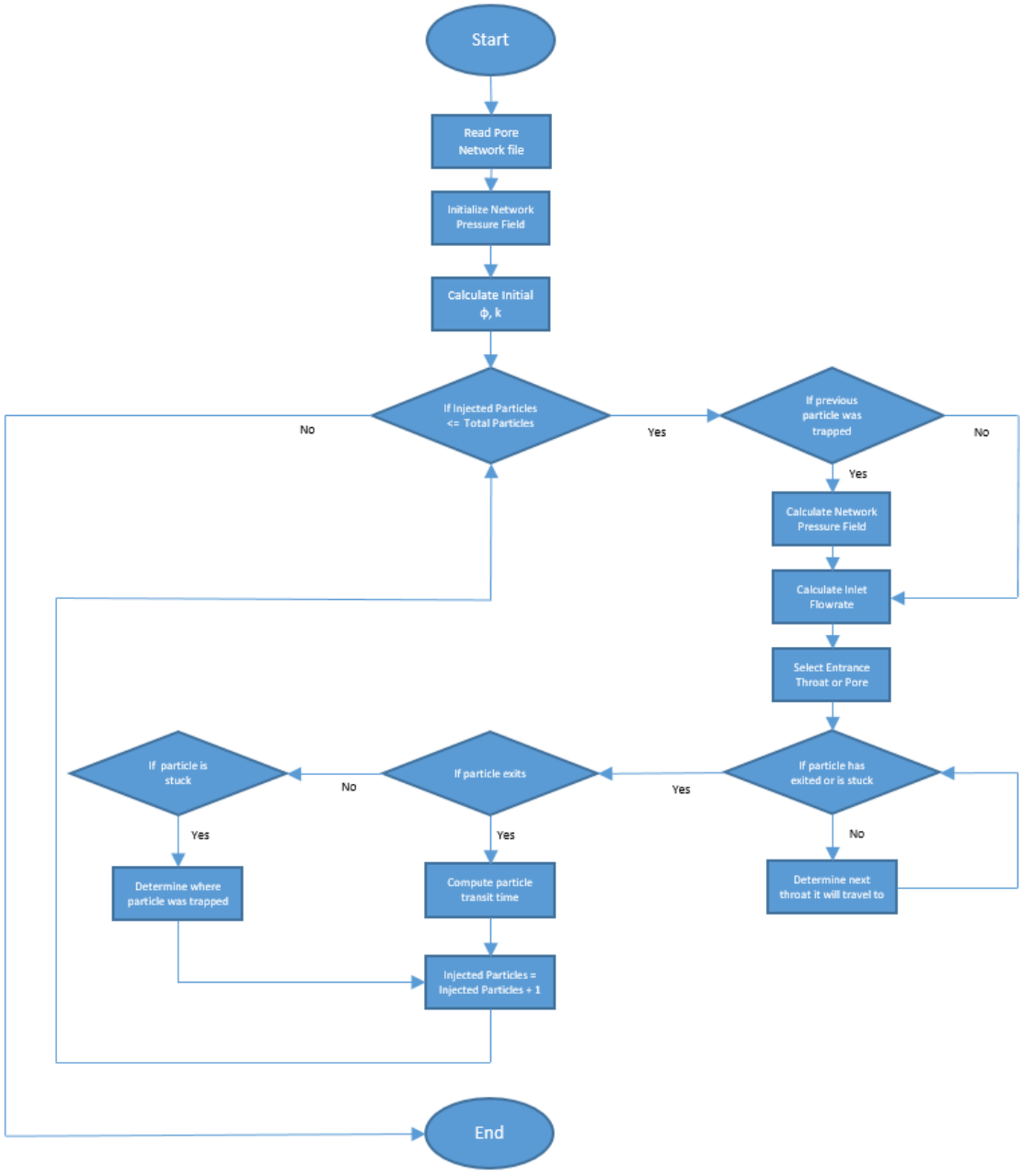

Figure 27: Particle plugging simulator flowchart.

VITA

Layne French received his Bachelors of Science in Geosystems Engineering and Hydrogeology from the University of Texas at Austin in 2013. He began his research with Dr. Thompson at Louisiana State University in the spring of 2014. Layne's academic interests include reservoir simulation, production system analysis, and computer programming. Layne is starting his career as a reservoir engineer with Marathon Oil Corporation in Oklahoma City, Oklahoma.